C.P. No. 1265

C.P. No. 1265

MINISTRY OF DEFENCE (PROCUREMENT EXECUTIVE)

AERONAUTICAL RESEARCH COUNCIL

CURRENT PAPERS

The Calculation of Compressible Turbulent Boundary Layers with Fluid Injection

By

L. C. Squire and V. K. Verma,

Cambridge University Engineering Department

LONDON: HER MAJESTY'S STATIONERY OFFICE

1973

PRICE £1 NET

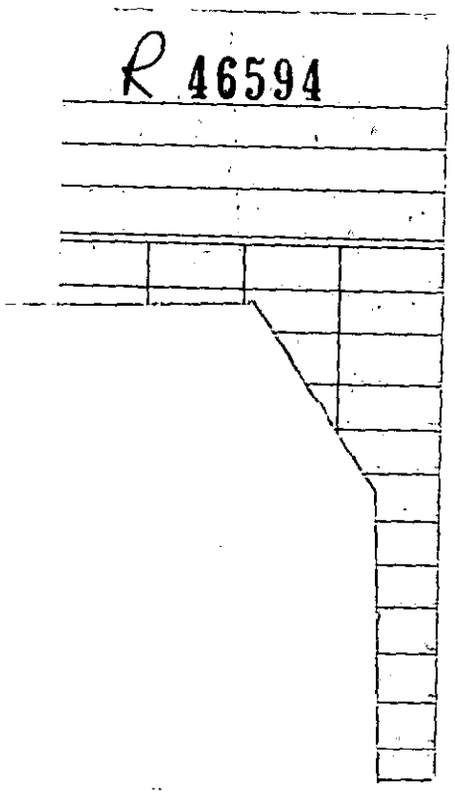
R 46594

CP No. 1265*
April, 1973

THE CALCULATION OF COMPRESSIBLE TURBULENT BOUNDARY LAYERS WITH FLUID INJECTION

- by -

L. C. Squire and V. K. Verma,

Cambridge University Engineering Department

SUMMARY

This paper presents the results of a large number of calculations for flat-plate turbulent boundary layers with heat transfer and fluid injection at Mach numbers up to 6.5. These calculations are based on various forms of eddy viscosity distribution. The paper also presents the results of a survey of most of the experimental data on layers with fluid injection.

In comparing the calculated and experimental results emphasis has been placed on well established correlations, such as the law of the wall, the law of the wake and the Reynolds analogy factor. In spite of the scatter in the experimental data, particularly in the case of injection, it has been found that the eddy viscosity model suggested by Cebeci gives the best overall agreement with experiment at all Mach numbers.

The authors believe that, although efforts should be made to improve the calculation methods, the main requirement at the moment is for better experimental data.

---

*Replaces A.R.C.34 503

1 Introduction

In conjunction with an extensive experimental study of compressible turbulent boundary layers with fluid injection we have developed a prediction method[1] to deal with this type of flow. This method uses an eddy viscosity model for the Reynolds stress terms in the boundary layer equations and a constant turbulent Prandtl number to model the corresponding terms in the energy equation. The prediction method is similar to that developed by Cebeci and Smith[2], and in most of the calculations we have used an eddy viscosity distribution of the same form as suggested by these authors. In general the agreement between experiment and prediction is good. However, during the investigations it was found that the predicted results did not agree with certain features of the experimental results. In particular it was found that the predicted profiles for compressible flows on solid surfaces in zero-heat-transfer conditions did not collapse onto a single law of the wall when plotted in the co-ordinates suggested by Van Driest[3] and by Fenter and Stalmach[4]. Further, at low speeds with injection there are wide variations in the skin-friction results as obtained by various workers. These variations in skin friction lead to different laws of the wall and hence suggest a range of possible eddy viscosity models for use with injection.

In view of these discrepancies and difficulties we have undertaken a survey of the experimental data with injection, and have made calculations with a range of eddy viscosity models. The results of these computer studies, together with the analysis of the experimental results are discussed in this paper. In particular the effects of variations in the constants in the eddy viscosity models are presented in detail. It appears that for flows on solid surfaces, the effect of Mach number on the law of the wall plotted in Van Driest coordinates can be more or less eliminated by slightly adjusting the eddy viscosity model. Unfortunately, the uncertainties in the experimental data with injection at both low speeds and at high Mach numbers makes it impossible to draw firm conclusions about the actual eddy viscosity model to be used. However, it is shown that the present model is capable of predicting the overall trends of the experimental results with injection at Mach numbers up to 6.5. It is also hoped that results presented for different models may be of value as more experimental results become available.

It should be emphasised that although the method has been used successfully elsewhere to calculate flows with pressure gradients and with

discontinuous changes in surface injection rate, we are only concerned here with essentially equilibrium flows. Our object is to find a suitable eddy viscosity model which can deal with the effects of injection in equilibrium flows at all speeds and which also gives acceptable results in the absence of injection. Once such a model is established then the possible need to use some type of rate equations in non-equilibrium flows can be considered.

2. Outline of the present prediction method

A full description of the prediction method used in the present work, together with a copy of the program in FORTRAN IV is given in Ref. 1. Basically the method considers the boundary layer equations in the form:*-

$$\frac{\partial}{\partial x}(\rho u) + \frac{\partial}{\partial y}(\rho v + \overline{\rho' v'}) = 0 \qquad (1)$$

$$\rho u \frac{\partial u}{\partial x} + (\rho v + \overline{\rho' v'}) \frac{\partial u}{\partial y} = - \frac{dp}{dx} + \frac{1}{R_s} \frac{\partial}{\partial y} \left\{ \mu (1 + \frac{\nu_t}{\nu}) \frac{\partial u}{\partial y} \right\} \qquad (2)$$

$$\rho u \frac{\partial H}{\partial x} + (\rho v + \overline{\rho' v'}) \frac{\partial H}{\partial y} =$$

$$\frac{1}{R_s} \frac{\partial}{\partial y} \left\{ \frac{\mu}{P_r} \left[(1 + \frac{P_r \nu_t}{P_{rt} \nu}) \frac{\partial H}{\partial y} - T \frac{\partial c_p}{\partial y} + E_s ((P_r - 1) + \frac{P_r \nu_t}{P_{rt} \nu} (P_{rt} - 1)) u \frac{\partial u}{\partial y} \right] \right\} \qquad (3)$$

where the various quantitites have been non-dimensionalised with respect to properties at a reference stagnation point, s, a length scale δ_o and a velocity scale u_o and the following definitions are used:-

---

* In the original formulation of the method, and in the method used by Cebeci and Smith, the term $E_s \frac{P_r \nu_t}{P_{rt} \nu} (P_{rt} - 1) u \frac{\partial u}{\partial y}$ did not appear since P_{rt} was defined as $- \nu_t \frac{\partial H}{\partial y} / (\overline{H' v'})$ instead of $- \nu_t \frac{\partial h}{\partial y} / (\overline{h' v'})$ as used in the present calculations. In future work in this paper the original definition will be referred to as P_{rT}. The effects of the two definitions are discussed in section 3.4 and in appendix B.

$$R_s = \frac{u_o \delta_o}{\nu_s} \quad , \text{ a reference Reynolds number} \tag{4}$$

$$E_s = \frac{u_o^2}{H_s} \quad , \text{ a reference Eckert number} \tag{5}$$

$$\nu_t = -\overline{u'v'} / \frac{\partial u}{\partial y} \tag{6}$$

$$k_t = -\overline{h'v'} / \frac{\partial h}{\partial y} \tag{7}$$

$$P_{rt} = \nu_t / k_t \tag{8}$$

Elimination of the term $(\rho v + \overline{\rho' v'})$ by the introduction of a stream function and the use of various transformations reduce the equations to a form suitable for numerical integration. These transformed equations are then reduced to a set of simultaneous equations for the values of u and T at each grid point in the y direction by an implicit finite difference scheme. The resultant set of equations are then solved by a standard diagonal matrix inversion scheme subject to the appropriate boundary conditions. The solution is an iterative scheme in that the equations for u are solved first, and the results used to solve for T. The cycle continues until convergence is obtained.

The main point of interest in the present study is the form used for the eddy viscosity defined by eqn. (6). The form used is basically the same as that suggested by Cebeci and Smith. In the inner region it has the form

$$\nu_t = \kappa^2 y^2 \left[1 - \exp(-y^+/A)\right]^2 \left|\frac{\partial u}{\partial y}\right| \tag{9}$$

where the damping length A is given by

$$A = A_o \left\{ -\frac{p^+}{v^+} \left[\exp(11.8v^+) - 1\right] + \exp(11.8v^+) \right\}^{-\frac{1}{2}} \tag{10}$$

In these equations κ is the von Karman constant, usually taken as 0.4, and A_o is the van Driest damping factor for a flat plate in incompressible flow with zero mass transfer. For $\kappa = 0.4$, A_o has the value 26. p^+, v^+ and y^+ are given by

$$p^+ = -\frac{dp}{dx} \cdot \frac{\nu}{\rho_w u_\tau^3} \quad , \quad y^+ = \frac{y u_\tau}{\nu_w} \quad \text{and} \quad v^+ = \frac{v_w}{u_\tau} \quad ,$$

where $u_\tau = (\tau_w/\rho_w)^{\frac{1}{2}}$. In these definitions ν is the local kinematic

viscosity. It should be noted that Cebeci and Smith define u_τ in eqn (9) in terms of the local density, rather than the wall density as used here. The effect of this change will be discussed below.

In the outer region the eddy viscosity is given by

$$\nu_t = c_o u_1 \delta_k^x (1 + 5.5 (y/\delta_{o.999})^6)^{-\frac{1}{2}} \tag{9A}$$

where $\delta_k^x = \int_o^\delta (1 - \frac{u}{u_1}) dy$. In most of the calculations c_o has the value 0.0168. However, the actual value to be used is discussed below.

3 Results on solid surfaces

3.1 Law of the Wall

In the past there have been a number of suggestions for the law of the wall for compressible boundary layers on solid surfaces. One of the most successful has been that suggested by van Driest. This law is based on the assumption of a constant shear stress near the wall and a mixing length assumption of the form

$$\tau = \rho \kappa^2 y^2 \frac{\partial u}{\partial y} \left| \frac{\partial u}{\partial y} \right| \tag{11}$$

These assumptions suggest replacing u/u_τ in the incompressible law by u^x/u_τ , where

$$u^x = \int_o^u (\frac{\rho}{\rho_w})^{\frac{1}{2}} du . \tag{12}$$

For constant stagnation temperature flows ρ/ρ_w can be replaced by

$$\frac{T_{o1}}{T} = 1 \Big/ (1 + \frac{T_1 - T_{o1}}{T_{o1}} (\frac{u}{u_1})^2) ,$$

so that

$$\frac{u^x}{u_1} = \frac{1}{\sigma^{\frac{1}{2}}} \sin^{-1}(\sigma^{\frac{1}{2}} \frac{u}{u_1}) , \tag{13}$$

where

$$\sigma = \frac{\gamma - 1}{2} M_1^2 \Big/ (1 + \frac{\gamma - 1}{2} M_1^2) . \tag{14}$$

3.1.1 Zero Heat Transfer

For flows with zero heat transfer the static temperature distribution through the layer can be approximately replaced by

$$T = T_r - (T_r - T_1)(\frac{u}{u_1})^2 ,$$

where T_r is the recovery temperature given by

$$T_r = T_1(1 + r\frac{\gamma - 1}{2}M_1^2),$$

so that σ in eqns. (13) and (14) is replaced by

$$\sigma_1 = r\frac{\gamma - 1}{2}M_1^2 \quad (1 + r\frac{\gamma - 1}{2}M_1^2). \qquad (15)$$

However, in the inner part of the layer ($y^+ < 400$) the change from σ to σ_1 produces a change of at most 0.5 % in u^x/u_1 for values of M_1 less than 5.

Using the transformation given by eqns. (13) and (14) Fenter and Stalmach[4] showed that for Mach numbers between 1.7 and 3.7 and for values of R_θ from 3,000 to 13,000, the law of the wall could be written as

$$\frac{u^x}{u_\tau} = \frac{1}{\kappa}\ln\frac{u_\tau y}{\nu_w} + B, \qquad (16)$$

where $u_\tau = (\tau_w/\rho_w)^{\frac{1}{2}}$ and ν_w is the kinematic viscosity at the wall temperature. Furthermore, they found that the values of κ and B were independent of Mach number and were close to the low speed values. This conclusion has since been confirmed by a number of authors and a set of the latest results of Mabey[5] for Mach numbers of 2.5, 3.5 and 4.5 at values of R_θ from 7,000 to 28,000 are shown in Figure 1.

During the present investigation the temperature distribution was found directly from the solution of the energy equation and u^x was obtained by direct integration of eqn. (12). At fixed Mach number the law of the wall so obtained was independent of R_θ (typically in the range 5,000 to 50,000) but the parameter B in eqn. (16) decreased with increase in Mach number. Typical results are shown in Figure 2. The top set of results show the law of the wall, i.e. u^x/u_τ plotted against $\ln(u_\tau y/\nu_w)$, for Mach numbers from 0 to 5. These results were obtained using the constants $\kappa = 0.4$, $A_o = 26$ and $c_o = 0.0168$. As will be seen the values of u^x/u_τ at $u_\tau y/\nu_w = 100$ decrease from 16.7 at M = 0 to 15.6 at M = 5. As a check, the values of u^x/u_τ at $u_\tau y/\nu_w = 100$ were also calculated from eqn. (13) with σ given by eqns. (14) and (15). The recalculated values were in close agreement with the computed values, for example, at M = 5 the values of u^x/u_τ were 15.57 (eqn.(14)) and 15.53 (eqn.(15)).

The effect of Mach number on the predicted value of B depends upon the value of A_o and whether local or wall values of ρ and ν are used in eqns. (9) and (10). As pointed out in § 2 the above results were obtained

by defining u_τ as equal to (τ_w/ρ_w) in eqns.(9) and (10) whereas Cebeci and Smith use local density in the definition of u_τ. A number of calculations were made at M = 4.5 with the two definitions of u_τ and typical results are plotted in the second figure of Figure 2. As will be seen the use of local density raises the level of the law by about 0.3, but the result is still below the incompressible law, also the approach to the linear part of the curve is delayed to slightly higher values if y^+ as compared with the present method.

In a similar approach to that used here Bushnell and Beckwith[6] use wall values of ρ and ν in the damping function, i.e. eqn (9) becomes

$$\nu_t = \kappa^2 y^2 \left[1 - \exp\left(- \frac{y\sqrt{\tau_w/\rho_w}}{26\,\nu_w} \right) \right]^2 \left| \frac{\partial u}{\partial y} \right| \qquad (17)$$

It was found that use of the wall values in this form raised the level of the law close to the incompressible level. However, the approach to the linear part of the curve was delayed to $y^+ = 60$ compared to $y^+ = 30$ in the present method. The reason for this behaviour can be seen by considering the damping term in more detail. In the present method we use

$$\left[1 - \exp\left(\frac{-y\sqrt{\tau_w/\rho_w}}{26\,\nu} \right) \right]^2 = \left[1 - \exp\left(\frac{-y^+}{26\,\nu/\nu_w} \right) \right]^2 \qquad (18)$$

whereas Cebeci and Smith use

$$\left[1 - \exp\left(\frac{-y\sqrt{\tau_w/\rho}}{26\nu} \right) \right]^2 = \left[1 - \exp\left(- \frac{y^+}{26\,\frac{\nu}{\nu_w}\left(\frac{\rho}{\rho_w}\right)^{\frac{1}{2}}} \right) \right]^2 \qquad (19)$$

and Bushnell and Beckwith use

$$\left[1 - \exp\left(- \frac{y^+}{26} \right) \right]^2 \qquad (20)$$

where $y^+ = y(\tau_w/\rho_w)^{\frac{1}{2}}/\nu_w$ in all cases. Taking $\mu \sim T^{0.9}$ it will be seen that the damping length increases from $26(T/T_w)^{1.9}$, through $26(T/T_w)^{1.4}$ to 26 for the three cases. Thus the increase in the level of the law is associated with the increase in damping length. However, near the wall $(T/T_w) = 1$, so the main increase takes place away from the wall. In order to get an earlier approach to the linear region and to raise the level of the law a calculation was made with the damping constant increased from 26 to 30 in eqn.(18). The resultant curve is close to the

incompressible law, and the linear region extends to lower values of y^+ than does the law at M = 0. Since Mabey's results (Figure 1) show this earlier approach to the logarithmic region it may be best to increase A_o rather than use the values of both ρ_w and ν_w rather than local values. However, it must be pointed out that the experimental values near the wall may be affected by probe interference effects and so it is difficult to draw firm conclusions on this point.

Further examples of the effects of changes in the constants κ and A_o on the law of the wall are shown in the lower figure of Figure 2. The effects of these changes on skin friction will be discussed below.

3.1.2 With Heat Transfer

The results discussed so far apply to the case of zero heat transfer where it is generally agreed that the law of the wall in van Driest co-ordinates is independent of Mach number. For the case of heat transfer the earlier experimental evidence for the law of the wall is less clear, and there is a large amount of scatter in the experimental results. This scatter can be attributed to three main causes: (i) the lack of accurate skin-friction data (ii) the fact that in deriving u^x (eqn. (12)) the static temperature has been taken as $T = T_w + (T_r - T_w)\frac{u}{u_1} + (T_r - T_1)(\frac{u}{u_1})^2$, whereas in many of the experiments the measured temperatures near the wall are not in agreement with the relation, and (iii) many of the experimental results with heat transfer are at low Reynolds numbers and there is some doubt as to whether the flow is fully turbulent (see Fernholz[7]). However, most of the data does suggest that the mixing length constant is independent of heat transfer, whereas the additive constant B increases with heat transfer to the wall, i.e. in the cold wall case. For example, at a Mach number of about 6.5 and R_θ of about 5,000, Danberg[8] found that the additive constant increased from 6.3 to 10 as the wall was cooled from $T_w/T_1 = 7$ to $T_w/T_1 = 4.3$ (note that the adiabatic wall temperature is about 8.5 T_1). A series of calculations were made using the present computer programmes to study the effect of heat transfer on the law of the wall. Again u^x was found by integration using the density ratio found from the calculated temperature profiles. Typical results are shown in Figure 3 and 4. Figure 3 shows the calculated results compared with the results of Danberg mentioned above. As will be seen, the calculated results give higher skin-friction coefficients than those found by Danberg, hence the overall level of the wall is lower. Since

the discrepancy for the skin-friction coefficients is greatest for the cold wall case the change in the level of the wall law with cooling is much smaller in the calculations. It is also interesting to note that Danberg's data lies close to the calculated wall-law when based on the calculated skin-friction. The fact that Danberg's measured skin-friction is too low is confirmed by the recent measurements of Hopkins et al[9] (see Figure 22). In fact their measured profiles show very little effect of heat transfer in Van Driest coordinates.

Figure 4 shows a similar set of predicted results for M = 4.5 at a Reynolds number of 16,000. As will be seen the effect of cooling the wall from $T_w/T_1 = 0.93$ to 0.3 is to increase the level of the wall-law by about 1.0 while the skin-friction coefficients were increased by about 0.0004.

The calculated results were also compared with a new correlation recently suggested by Winter and Gaudet [10]. This correlation is of the form

$$\frac{u}{u_\tau^i} = 6.05 \log \frac{y\, u_\tau^i}{\nu_1} + 4.05$$

where $u_\tau^i = u_1 \left(\frac{c_f}{2} (1 + 0.2M_1^2)^{\frac{1}{2}} \right)^{\frac{1}{2}}$, and ν_1 is the kinematic viscosity at the outer edge of the layer. Again the basic calculated results at fixed R_θ showed the same trends as in Figure 2, i.e. the level of the logarithmic region fell with increasing Mach number, and again better agreement could be obtained by using wall values of ρ and ν in the damping function, or by increasing A_o. A study of the relationship between the Winter and Gaudet law and the Fenter and Stalmach law is given in Appendix 1.

3.2 Law of the wake

As mentioned in § 2 the eddy viscosity in the outer region of the boundary layer is given by

$$\nu_t = c_o u_1 \delta_K^* \left(1 + 5.5 \left(y/\delta_{0.999}\right)^6\right)^{-\frac{1}{2}}$$

where c_o is taken as a constant independent of Reynolds number and Mach number. Experimental justification for a universal form of eddy viscosity was first obtained by Maise and McDonald[11] who analysed a set of experimental results on solid surfaces with zero heat transfer. From their analysis they found that the results could be expressed in terms of a universal velocity-defect law in van Driest coordinates. Calculation of

shear stress and hence eddy viscosity from this defect law lead to an eddy viscosity distribution of the form given above, i.e. ν_t is directly proportional to the product $u_1 \delta_K^x$. In an analysis of more experimental data, both Squire[12] and Fernholz[7] found a large amount of scatter in the magnitude of the wake function in van Driest coordinates. For supersonic speeds the main level was about 3.4, i.e. slightly larger than the corresponding value of 2.7 at low speed. As a result of his analysis Squire suggested that the constant c_o may decrease slightly with Mach number, although it appears to be independent of injection at fixed Mach numbers. In view of this suggestion a number of calculations were made with different values of the constant c_o. A typical set of results are shown in Figure 5, where u^x/u_τ is plotted against y^+. As will be seen the size of the wake function is almost independent of $R_\theta (5000 < R_\theta < 50{,}000)$ for fixed c_o, but the strength of the wake function decreases with increase in c_o. All the calculated results are summarised in Figure 6, and it is interesting to note that the strength of the wake function in van Driest co-ordinates is virtually independent of Mach number for $c_o = 0.0168$. Furthermore, the strength is almost the same as the mean value found by Squire and Fernholz.

It should be noted here that the types of plots used in Figures 1 - 6 have been chosen to highlight small differences, in fact if the profiles are plotted in normal co-ordinates (say, u/u_1 against y/θ) then the effects of the variation in A_o, κ and c_o are relatively small. This is illustrated in Figure 7 where a set of results are presented for M = 2.5. The left-hand set of curves show the various calculated profiles while the right-hand curve shows a set of results measured by Mabey[5] compared with the extremes of the calculated profiles. On the scales used in most published papers any of the calculated curves would appear to be in good agreement with the experiments.

3.3 Skin-friction results

The basic program ($\kappa = 0.4$, $A_o = 26$, $c_o = 0.0168$) was used to calculate skin-friction coefficients for a range of Mach numbers and Reynolds numbers in zero-heat-transfer conditions. In all cases the computed values were within 0.00003 of the calculated values quoted by Cebeci[13]. In this reference Cebeci showed excellent agreement between his calculated values and the corresponding measured values. Of more interest in the present study is the effect of changes in the eddy

viscosity parameters. Turning first to the effects of changes in the eddy viscosity distribution near the wall, i.e. in κ and A_o, it was found that the value of the skin-friction coefficient was directly related to the level of the law of the wall. Thus any combination of changes in κ and A_o which gave the same level of the law of the wall also gave virtually the same skin-friction coefficient. This is illustrated in Figure 8 for a set of computed results at M = 2.5; the related changes in the law of the wall are shown in Figure 2. In general the magnitude of the increment in the skin-friction coefficient for a corresponding increment in the level of the law of the wall was almost independent of Mach number.

The corresponding changes due to the level of the eddy viscosity in the outer region are also shown in Figure 8. Again the changes were almost independent of Mach number.

Figure 8 also compares these results with various measured skin-friction coefficients at M = 2.5. (These points were measured at Mach numbers between 2.4 and 2.6, and the theoretical variation of c_f with M at constant R_θ was used to correct all the measured points to a Mach number of 2.5. All the results plotted in Figure 8 are tabulated in Table 1 and it will be seen that the maximum correction is 0.00003.) Figure 8 shows that the scatter in the experimental results is almost as great as the spread of the various computed curves. The only definite conclusion that can be drawn is that the value of c_o should not be much greater than 0.0168.

3.4 Temperature results

In most of the early work on flat-plate turbulent boundary layers with heat transfer it has been assumed that the total temperature distribution is approximately given by the result obtained when $P_{rt} = P_r = 1$.

In this case $\dfrac{H - H_w}{H_1 - H_w}$ or $\dfrac{T_o - T_w}{T_{o1} - T_w}$ satisfies the same equation and boundary conditions as u/u_1. So that

$$T_o = T_w + (T_{o1} - T_w)(u/u_1) \qquad (21)$$

Near adiabatic conditions this approximation is obviously in error and so eqn.(21) is modified to

$$T_o = T_w + (T_r - T_w)(u/u_1) + (T_{o1} - T_r)(u/u_1)^2, \qquad (22)$$

since this relationship gives $T_o = T_w$ at $u = 0$, $T_o = T_{ol}$ at $u = u_1$ and zero heat transfer when T_w equals the recovery temperature.

Figure 9, shows a set of calculated total temperature profiles plotted against u/u_1 for $M = 4.5$ with various wall temperature ratios. Near adiabatic conditions ($T_w/T_{ol} = 0.92$ for $r = 0.9$) results calculated with $P_{rt} = 0.9$ show that there is a slight heat transfer from the wall, but this disappears if T_w/T_{ol} drops to 0.913, (i.e. $r = 0.89$). Near the wall the calculated total temperature is close to that given by eqn. (22), but in the outer part of the layer a distinct overshoot appears, as in fact must exist to give zero enthalpy flux in the layer. Results were also calculated with $P_{rT} = 0.9$ as used by Cebeci and Smith. In this case there is considerable heat transfer to the wall and there is very little overshoot in the outer part of the layer. As shown in Appendix B, a value of $P_{rt} = 0.9$ corresponds in these conditions to value of P_{rT} which tends to infinity so it is not surprising that the calculated profiles are different. The figures also show an empirical result deduced by Winter and Gaudet from published experimental data. This result is given in the form

$$\frac{\frac{1}{T} - \frac{1}{T_w}}{\frac{1}{T_1} - \frac{1}{T_w}} = 0.975 \left(\frac{M}{M_1}\right)^2$$

and was based on data obtained in the outer part of the layer, (i.e. $u/u_1 > 0.6$). The present results are in fair agreement with this result for the inner and outer parts of the layer, particularly near the inner part of the over-shoot region. (The empirical result breaks down right at the edge since T_o does not return to T_{ol}.)

Results were also calculated for $T_w/T_{ol} = 0.7$ and 0.3 with $P_{rt} = 0.9$. In both cases the calculated total temperature is slightly below eqn.(22) near the wall and tends to the linear relation (eqn.(21)) at the outer edge. This trend is in agreement with all the experimental data, which shows a linear variation of T_o/T_{ol} with u/u_1 for boundary layers on flat plates. In general results have only been obtained for values of $u/u_1 > 0.5$ so that no comparison with experiment for the inner region is possible. In both

cases the calculated Reynolds analogy factor $\frac{2\,S_t}{c_f}$ is just over 1.1 (similar values were found in other calculations at higher Mach numbers). This value is in close agreement with measured values which appear to show a mean value of 1.15, although some recent results by Keener and Polek[14] for $T_w/T_{ol} = 0.3$ at Mach numbers between 6 and 8 suggest a mean value of 1.0. In view of the scatter in the experimental data the present method with $P_{rt} = 0.9$ which gives $r = 0.89$ and $2\,S_t/c_f \doteq 1.12$ appears satisfactory.

Two further calculations were made for $T_w/T_{ol} = 0.7$ with $P_{rT} = 0.9$ and 1.2. As will be seen the variations of T_o through the layer is similar to that obtained with $P_{rt} = 0.9$. In fact with $P_{rT} = 1.2$ the results are almost identical to those for $P_{rt} = 0.9$, (with $2\,S_t/c_f = 1.11$ compared with 1.14 for $P_{rt} = 0.9$). However, for $P_{rT} = 0.9$ the heat transfer at the wall is higher, corresponding to $2\,S_t/c_f = 1.29$. The agreement between the results with $P_{rT} = 1.2$ and $P_{rt} = 0.9$ can be explained by the results considered in Appendix B, where it is shown that for $P_{rt} = 0.9$, P_{rT} under these conditions, varies from 0.9 at the wall to about 1.9 at the edge of the layer. However, results with $P_{rT} = 0.9$ would appear to give too high heat transfer rates.

Figure 10 show typical results for higher Mach numbers. Of particular interest here is the lower figure which shows calculated results with high heat transfer and a high injection rate. The shape of the curve is similar to that without injection, but the Reynolds analogy factor is now 1.3 compared with 1.12 without injection. (In calculating the Stanton number it has been assumed that the recovery temperature is independent of injection).

Figure 11 shows the effect of errors in the initial profile, in this case the calculations were started using a measured temperature distribution. The temperature recovers to a profile close to that given by eqn. (22) in about 4 boundary layer thicknesses.

4. Layers with injection

In the last section it has been shown that it is possible to extend the incompressible eddy viscosity distribution to compressible flow with only minor modifications to the damping function. Turning to the cases of layers with injection the main problem is the form of the eddy viscosity to be used in incompressible flow. This extension is complicated by the fact that a number of authors have made measurements of layers with injection and although they get good agreement with each other in measured velocity profiles in the form of u/u_1 against y/θ at the same R_θ and v_w/u_1, they get widely different skin-friction coefficients (Figures 12 and 13). This variation in the measured skin-friction coefficient leads to different wall laws, and hence to different damping functions in the eddy viscosity. Thus before considering any extension to compressible flow it is first necessary to consider the low speed data in more detail. In fact the low speed data is now the key to the whole problem since with injection most of the damping takes place at values of y^+ less than 10 where the velocity is low, and hence, where even at high Mach numbers, the temperature variations are small. Thus the damping takes place in a region which is effectively at constant (wall) temperature.

4.1 Law speed data and law of the wall

The skin-friction data obtained by various workers 15-19 is presented in Figures 12 and 13. In assessing these results it must be remembered that all of these results, except those of Anderson[19] were obtained by indirect methods, usually from the momentum integral equation. This method in whatever guise it is used is basically inaccurate especially

at the higher blowing rates where the skin-friction is the small difference of two large quantities both of which are subject to error. Anderson's results were obtained in the same tunnel as used by Simpson[16], However, Anderson measured mean velocities and shear stress by hot wires and found the skin-friction by extrapolating the measured shear stress back to the surface. It is interesting that his results are significantly lower than those of Simpson. It should also be noted that all the results are for relatively low Reynolds numbers and that the discrepancies between the various sets of results also exist for zero injection where the momentum equation should be relatively accurate. This is shown in Figure 14 where it can be seen that the results quoted by Simpson[16] are significantly higher than those obtained by McQuaid[15] and Anderson, while the results of Kendall et al[17] and of Baker[18] lie between the two extremes. The figure also includes the skin-friction laws for solid surfaces as proposed by Coles[20,21]. In the light of Coles[21] remarks that he has some reservations about his skin-friction laws for $Re < 6{,}000$ it is difficult to decide which of the experimental results is likely to be correct,although Anderson's method of finding skin-friction should be the most accurate. In a re-analysis the results of McQuaid and Simpson by Squire[22] it has been concluded that (a) the differences between the two sets of data cannot be explained in terms of analysis used and (b) both sets of results have certain inadaquacies which makes the choice between them difficult. Since this re-analysis was completed some of McQuaid's results have been checked by a different worker who obtained almost identical results to McQuaid. On the other hand Coles[23] in a study of all the low speed data has concluded that Simpson's skin-friction results lead to the most satisfactory law of the wall, though this conclusion was reached before publication of Anderson's results.

Turning to the actual law of the wall in incompressible flow there have been a number of suggestions. Based on his own work, and the early experimental results of Mickley and Davies[24], Stevenson[25] proposed the law

$$\frac{2}{v^+}\left((1 + u^+ v^+)^{\frac{1}{2}} - 1\right) = \frac{1}{\kappa} \ln y^+ + B, \qquad (23)$$

where $v^+ = v_w/u_\tau$, $u^+ = u/u_\tau$, $y^+ = yu_\tau/\nu_w$ and $u_\tau = (\tau_w/\rho_w)^{\frac{1}{2}}$. He further found that the constants κ and B were independent of injection and so could be given the Coles values of 0.41 and 5.0 respectively. From the analysis of his own results Simpson[16] again found that κ was independent of injection rate, although he found that it had an average value of 0.44. However, his wall-law, when expressed in Stevenson's form, shows that B strongly depends on v^+ and is given by

$$B = \frac{2}{v^+}\left((1 + 11v^+)^{\frac{1}{2}} - 1\right) - \frac{1}{\kappa} \ell n\ 11 \ . \qquad (24)$$

Following these empirical approaches there have been a number of theoretical methods based on eddy viscosity or mixing length. For example Kendall et al.[17] used an extended mixing length approach to derive a numerical law in the form $u^+ = f(y^+, v^+)$. Re-arranging their numerical results in Stevenson's form again shows that κ is independent of injection, but that B now decreases slowly with v^+, although the rate of decrease is much slower than that found by Simpson. Kays[27], Cebeci and Smith, Michel[26], Baker[18] and Bushnell have all approached the logarithmic region via eddy viscosity. Essentially all these authors assume that the eddy viscosity is given by

$$\nu_t = \left(1 - \exp\left(-\frac{y^+}{A_o}\right)\right)^2 \kappa^2 y^2 \left|\frac{\partial u}{\partial y}\right| \ , \qquad (25)$$

where A_o is now a function of v^+ and u^+. They differ in the form of this function. On solid surfaces the damping length A_o is given by

$\frac{26\nu_w}{\sqrt{\tau/\rho_w}}$ or $\frac{26\nu_w}{\sqrt{\tau_w/\rho_w}}$ since τ is constant near the wall. With injection (or pressure gradient) τ is not constant near the wall and Michel, and Cebeci and Smith extend the first form of A_o by use of a suitable shear stress. This shear stress is found by a Couette flow analysis. Thus, in the absence of pressure gradient, the boundary layer equations in this approximation can be written

$$\frac{\partial}{\partial y}(\rho v) = 0, \text{ or } \rho v = \rho_w v_w \qquad (26)$$

and

$$\rho_w v_w \frac{\partial u}{\partial y} = \frac{\partial \tau}{\partial y} \qquad (27)$$

so

$$\tau = \tau_w + \rho_w v_w u$$

or

$$\tau/\tau_w = 1 + v^+ u^+ \qquad (28)$$

Michel uses this result directly so that the damping function in the presence of injection becomes

$$\left(1 - \exp\left(-\frac{y^+}{26}\left(1 + u^+ v^+\right)^{\frac{1}{2}}\right)\right)^2 . \tag{29}$$

On the other hand Cebeci decided to evaluate τ at the edge of the sub-layer which he defined as $y^+ = 11.8$. To find τ at $y^+ = 11.8$ he put $\tau = \mu \frac{\partial u}{\partial y}$ in the sub-layer so that eqn (27) becomes

$$\frac{\rho_w v_w \tau}{\mu} = \frac{\partial \tau}{\partial y} \tag{30}$$

or $$\tau = \tau_w \exp(v^+ y^+)$$

so $$\frac{\tau}{\tau_w} = \exp(11.8\, v^+) \quad \text{at } y^+ = 11.8. \tag{31}$$

Thus the damping function is given by

$$\left(1 - \exp\left(-\frac{y^+}{26} \exp(5.9\, v^+)\right)\right)^2 \tag{32}$$

or by eqn. (10) if pressure gradient is included.

Kays and Baker originally used the damping function given by eqn (29). However, they found that this approach did not give good agreement with experiment so they allowed additional variation in A_o. Kays chose this variation so that the calculated values of u^+ at $y^+ = 100$ were equal to the experimental points as measured by Simpson. This approach lead to the damping function given by

$$\exp\left(-\frac{y^+\left(1 + v^+ u^+\right)^{\frac{1}{2}}}{26C}\right) ,$$

where

$$C = 5.15\left(v^+ + \frac{5.86}{1 + 5v^+}\right) + 1 \tag{33}$$

Baker obtained good agreement with his own data by using the damping function

$$\exp\left(-\frac{y^+(1 + v^+ u^+)}{26}\right)$$

i.e. by using τ/τ_w rather than $(\tau/\tau_w)^{\frac{1}{2}}$

Finally Bushnell and Beckwith found A_o (eqn 25) from the experimental data of Simpson and Kendall as the value of y^+ where data near the wall first deviates from a straight line in a semilog plot of u^+ against y^+. They expressed their results as a function of $(\rho_w v_w/\rho_1 u_1)/\frac{c_f}{2}$, rather than as a function of v^+. However, the trend of their damping function is similar to that found by Cebeci and by Kays. Although this method of finding A_o gives the same results from the two sets of data, it should be noted that the actual data differs considerably when plotted as u^+ against y^+. This is shown in Figure 15, where one profile from Kendall is compared with two profiles of Simpson, one at approximately the same value of v^+(= 0.122) and one at approximately the same value of $(v_w/u_1)/\frac{c_f}{2}$ (= 5.1). It will be seen that although all the results deviate from a straight line at about the same value of $y^+(12 \pm 2)$, the levels of the three curves are quite different.

The effects of these various damping functions on the velocity near the wall are shown in Figures 16-18. Figure 16 shows the results in Stevenson's co-ordinates as obtained using the damping functions of eqns (29), (32) and (33) and the results of Kendall for various values of v^+. All these results are summarised in Figure 17, where the value of u^+ at $y^+ = 100$ is plotted against v^+ and in Figure 18 where the results at $y^+ = 100$ are plotted in Stevenson's co-ordinates. The last two figures also include the empirical results of Stevenson (eqn. (23)) and Simpson (eqn (24)). As will be seen the results fall into two distinct groups. The methods of Michel and Kendall give little variation of the levels of the law of the wall in Stevenson's co-ordinates and conversely give a large variation in u^+ at $y^+ = 100$. On the other hand the results from the methods of Cebeci and of Kays do not collapse in Stevenson's co-ordinates but do give a much smaller variation of $u^+(y^+ = 100)$ with v^+. In the rest of this paper we will take the damping functions of Cebeci and of Michel as representative of the two groups. Figure 17 also includes the values of u^+ at $y^+ = 100$ as measured by Anderson. As mentioned above, Anderson's results were obtained with hot wires and his skin-friction was found from the measured

shear stress in the boundary layer. The bulk of Anderson's results lie mid-way between the empirical results of Stevenson and of Simpson, and the overall trend of the results is close to that predicted by the damping function used by Cebeci.

One interesting result in Figure 16 is that as blowing is increased the straight portion of the curve extends to lower values of y^+. Also the intersection of the extrapolated linear logarithmic region with the laminar sub-layer (which is given by $u^+ = \frac{1}{v^+}(e^{v^+y^+} - 1)$ also occurs at lower values of y^+ with increasing v^+. Since this intersection is taken as the edge of the sub-layer, Cebeci's assumption of a constant value of y^+ (= 11.8) at the edge of the sub-layer is obviously in error and hence so is the justification for his damping function. It should also be noted that, as pointed out by Coles, Simpson's law of the wall does not intersect the sub-layer for $v^+ > 0.4$.

On the other hand it must be pointed out that Cebeci's calculations do give much better agreement with the experimental results with respect to this trend of increasing logarithmic region to lower values of y^+. A study of the results of Simpson and McQuaid show a clear laminar sub-layer and blending region for $v_w/u_1 < 0.005$ with the logarithmic region moving to lower values of y^+ with increase in v^+, reaching $y^+ = 10$ at $F = 0.005$ ($v^+ \doteq 0.2$). For $v_w/u_1 = 0.008$, ($v^+ \doteq 0.6$) the experimental points lie on a straight line in semi-logarithmic co-ordinates down to $y^+ = 2$. This trend is in good agreement with the calculations based on the damping function used by Cebeci (Figure 16). However, use of the damping function suggested by Michel still gives a pronounced blending region for $y^+ > 10$. On these grounds it would seem that the damping function used by Cebeci is the more plausible.

In general, use of both damping functions gives good agreement with the measured boundary layer developments (θ and δ) of Simpson and McQuaid, and with the measured velocity profiles. However, the skin-friction coefficients for a given blowing rate predicted by the Cebeci type damping function tend to be higher than those predicted by use of the Michel type damping function. In fact Michel obtains excellent agreement with McQuaid's results (Figure 19). On the other hand, Cebeci gets much higher skin-friction coefficients, the actual values being

slightly lower than those measured by Simpson and higher than those measured by Anderson. It is this difference which allows both methods to give almost identical velocity profiles in physical co-ordinates, a characteristic which is shared by the experimental results. It should also be noted that Kays also obtains good agreement with measured heat-transfer-rate data obtained at Stanford.

The doubts expressed earlier about all the skin-friction data makes a final choice between the two types of damping function difficult. However, as will be shown later, the Cebeci type damping function does give much better agreement with results at supersonic Mach numbers. This fact, together with the more plausible behaviour near the wall at high blowing rates and the good agreement with Anderson's results suggests that the Cebeci type damping is the more realistic.

4.2 Compressible layers with injection

4.2.1 Law of the wall

In deriving his law of the wall for incompressible flow, Stevenson used the Couette flow results for shear stress together with the mixing length result

$$\tau = \rho \kappa^2 y^2 \left(\frac{\partial u}{\partial y}\right)^2$$

A similar approach in compressible flow leads to a wall law of the form (Squire[28] and Danberg[8])

$$\frac{u^{xx}}{u_\tau} = \int_0^u \frac{\rho^{\frac{1}{2}} \, du}{\sqrt{\rho_w \nu_w u + \tau_w}} = \frac{1}{\kappa} \ln \frac{y u_\tau}{\nu_w} + B(v^+). \qquad (35)$$

In the absence of injection this law reduces to the law proposed by van Driest (eqn (1)) while in incompressible flow it reduces to Stevenson's law. From this analysis of his own results at M = 1.8 and 2.5, together with Jeromin's results for M = 3.6 and Danberg's results for 6.7, Squire suggested that the parameter B decreases with increasing v^+, and that the rate of decrease increased with increasing Mach number. However, Squire presented his results in the form of $B(v^+) - B(v^+ = 0)$ (Figure 20) rather than directly as $B(v^+)$. It is now realised that the main reason for

the large change in $B(v^+)$ at $M \doteq 6.3$ is due to the high value of B at $v^+ = 0$. As has been shown in §3.2 this high value of B is not predicted by the present calculation method and is due to errors in Danberg's skin-friction coefficient. Figure 20 shows Squire's values of ΔB plotted against v^+, while Figure 21 shows the actual level of the law of the wall as typified by the value of u^{xx}/u_τ at $y^+ = 100$. In studying these two figures it must be remembered that the level of the wall law is very sensitive to the assumed skin-friction coefficient and that at the higher blowing rates the measured skin-friction coefficients could be in error by up to 100 %. In spite of these errors Figure 20 suggests that the slope of ΔB increases with increase in Mach number. On the other hand Figure 21 is less clear, and the only conclusion which can be drawn is that the level of the wall law decreases with injection. The influence of Mach number and heat transfer on the actual level is not clear.

4.2.2 Comparison of calculated and measured results

Calculations using the eddy viscosity distribution given by Eqns (9) and (10) have been made for comparison with the experimental results of Squire [29] at $M = 1.8$, Jeromin [30] at $M = 3.6$ and Danberg [31] at $M \doteq 6.3$. All these results are summarised in terms of the skin-friction coeffocients in Figure 22. Danberg obtained his skin-friction coefficients from the slope of the Mach number profile at the wall, whereas Squire and Jeromin used the momentum integral equation and so only obtained reliable results near the centre of the boundary layer development. At $M = 1.8$ and $M = 3.6$ the calculated and measured skin-frictions are in reasonable agreement, although at $M = 3.6$ the measured values are consistently higher than the calculated values. At $M = 6.3$ there is a lot of scatter in the data and the only consistent trend is shown by the fact that the calculated skin-friction with injection are always lower than the measured values. These differences have significant effects on the law of the wall. Figure 23 shows the calculated values of u^{xx}/u_τ (eqn (35)) at $y^+ = 100$ plotted against v^+ for $M = 0$, 1.8, 3.6 and 6.3. Except near $v^+ = 0$ the results collapse onto a single curve, this is in contrast to the experimental results (Figure 21) which show a lot of scatter in these co-ordinates. However, as pointed

out above, the calculated skin-friction with injection tended to be lower than the measured values for $M \geqslant 3.6$. In fact most of the scatter in Figure 21, is removed if the measured profiles are reduced to u^{xx}/u_τ using the calculated rather than the measured skin-friction coefficients. This is shown in Figure 24, where the measured profiles at the mid-station at $M = 1.8$ and $M = 3.6$ are compared with the calculated profiles in law of the wall coordinates. A similar comparison of u/u_1 against y is shown in Figure 25. At $M = 1.8$ the agreement between the measured and calculated profiles is excellent in both co-ordinates systems but at $M = 3.6$ there is a tendency for the measured velocities to be lower than the calculated values, particularly at the highest blowing rate.

It is more difficult to make meaningful comparisons with the data of Danberg, since there are a number of unexplained discrepancies in his measured temperature distributions. (An example of this is illustrated in Figure 27, where it can be seen that the static temperature appears to oscillate along the plate). One case where these discrepancies are small is for the cold wall case ($T_w/T_1 = 4.7$) at a stagnation pressure of 38 atmospheres with zero injection. A comparison of the calculated and measured results are shown in Figure 26. As will be seen the agreement between measured and calculated velocity and temperature profiles is excellent, as is the agreement on momentum development. However, the measured skin-friction coefficients are much lower than the calculated values. In this connection it should be noted that the measured values of c_f do not satisfy the momentum equation, and also that at slightly higher values of R_θ the calculated values are in excellent agreement with the skin-friction balance results of Hopkins et al (see Figure 22). It is also interesting that the measured values of Stanton number are approximately 50 % lower than the calculated values.

Figure 27 shows a similar set of results for a high injection rate ($F = 0.0025$) with high heat transfer. Although the momentum development is produced with good accuracy, as is the skin-friction and Stanton number, the calculated velocity tends to be lower than the measured velocity. Also the calculated temperature tends to be higher than the measured temperature. In view of the scatter in the measured temperature profiles it is difficult to draw firm conclusions from this comparison.

So while at M = 3.5 the calculated velocity is higher than the measured values the reverse is the case at M = 6.3. Thus there is no consistent trend in the results as Mach number increases.

Some calculations were also made using the Michel type of damping function. In general these calculations showed a worse agreement with experiment. In particular there was virtually no change in the level of the law of the wall with injection, and the skin-friction coefficients with injection were even lower than those obtained using the Cebeci type damping.

In summarising these results it should be noted that most of the experimental results with injection are not completely satisfactory. For example, Jeromins' data at M = 3.6 is known to be slightly three-dimensional while Danberg's data is at relatively low Reynolds numbers and there is some doubt if the layers are completely turbulent. In spite of these uncertainties the use of the Cebeci type damping function does give good overall agreement with the results. Certainly it predicts the general trend of the level of the law of the wall, and it gives skin-friction coefficients which are certainly in general agreement with the measured trends, although for M > 3.6 the theoretical skin-friction coefficients with injection tend to be lower than the measured values. Also, although there are some differences between the measured and calculated profiles, these differences have not been found to be systematic.

Finally Figure 28 shows the calculated skin-friction results plotted in the form c_f/c_{fo} against $2F/c_{fo}$, where c_{fo} is the calculated skin-friction on the solid surface at the same value of R_θ. It is interesting that all the results lie on a single curve so that the results show no effects of Mach number or heat transfer.

5. Conclusions

In earlier work on calculation methods most authors have made individual comparisons with a large number of experimental results. In this paper the emphasis has been placed on comparisons with established corellations of the experimental data, for example, law of the wall and wake and the Reynolds analogy factor.

For the solid surface it has been shown that the present method does give reasonable agreement with these experimental corellations at Mach numbers up to at least 6, although the agreement with the compressible law of the wall might be improved by allowing the damping length A_o to increase slowly with increase in Mach number. However, a final decision on this matter must await better experimental data.

With injection the comparisons are be-devilled by the scatter in the experimental data. However, a survey of all the available data together with the use of various damping functions appears to suggest that the use of the damping function given by Cebeci gives the best overall agreement with experiment at all speeds. Of course it may be possible to get better agreement with given sets of experimental data by use of other damping functions but the present authors believe that these modifications should await more reliable experimental data.

Appendix A

Comparison of the laws of the wall of van Driest and of Winter and Gaudet

As discussed in section 3.1 van Driest and Fenter and Stalmach have proposed a compressible law of the wall given by

$$\frac{u^x}{u_\tau} \equiv \frac{u_1}{u_\tau \sigma^{\frac{1}{2}}} \sin^{-1}\left(\sigma^{\frac{1}{2}} \frac{u}{u_1}\right) = \frac{1}{\kappa} \ln \frac{u_\tau y}{\nu_w} + B \qquad (A.1.1)$$

where κ and B have the same values as in incompressible flow, i.e. $\kappa = 0.41$ and $B = 5.1$. On the other hand Winter and Gaudet have proposed a law based on a transformation to a related incompressible flow, the resultant law is given by

$$\frac{u}{u_\tau^i} = 6.05 \log \frac{u_\tau^i y}{\nu_1} + 4.05 \qquad (A.1.2)$$

where $u_\tau^i = u_1 \left(\frac{c_f}{2}(1 + 0.2\,M^2)^{\frac{1}{2}}\right)^{\frac{1}{2}}$,

and ν_1 is the kinematic viscosity at the edge of the layer.

Van Driest's law was based on the assumption that the shear stress in logarithmic region was given by $\tau = \rho \kappa^2 y^2 \left|\frac{\partial u}{\partial y}\right|^2$ and that the density could be found from the temperature given by the Crocco relationship. In order to compare the two laws it is best to re-write them as a direct relationship for u/u_τ in terms of $\frac{u_\tau y}{\nu_w}$, where $u_\tau = (\tau_w/\rho_w)^{\frac{1}{2}}$. Thus A.1.1 becomes

$$\frac{u}{u_\tau} = \frac{u_1}{u_\tau \sigma^{\frac{1}{2}}} \sin\left(\frac{u_\tau \sigma^{\frac{1}{2}}}{u_1}\left(\frac{1}{\kappa} \ln \frac{u_\tau y}{\nu_w} + B\right)\right) , \qquad (A.1.3)$$

while A.1.2 becomes

$$\frac{u}{u_\tau} = \frac{u_\tau^i}{u_\tau}\left[6.05 \log \frac{u_\tau y}{\nu_w} + 6.05 \log \frac{u_\tau^i}{u_\tau}\frac{\nu_w}{\nu_i}\right] + 4.05 , \qquad (A.1.4)$$

Noting that $\sigma = \frac{\gamma - 1}{2} M_1^2 / (1 + \frac{\gamma - 1}{2} M_1^2)$, and that

$$\frac{u_\tau^i}{u_\tau} = 1/(1 + 0.2\,M^2)^{1/4} ,$$

it will be seen that A.1.4 is independent of skin-friction, i.e. of Reynolds number, and depends only on Mach number, where as A.1.3 also depends on c_f. The laws given by A.1.3 and A.1.4 are compared in Figure 29, for Mach numbers of M = 0, 1.66, 3.33 and 5.0. Results for the van Driest law are given for the values of R_θ of 6,000, 30,000 and 100,000. In comparing these results it should be remembered that $u_\tau \delta/\nu_w$ increases with R_θ and therefore that the outer edge of the logarithmic region extends to higher values of y^+ with increasing R_θ. In fact the van Driest laws are only drawn for the likely logarithmic region. At the lower Mach numbers the van Driest laws are almost independent of R_θ, biggest discrepancies between two laws occuring at the highest Reynolds numbers. On the other hand at Mach numbers above 3.0 the two laws are in very close agreement at the higher Reynolds numbers, (at R_θ = 30,000 the two laws are almost identical), whereas at the lower Reynolds numbers the van Driest law is significantly lower than the law proposed by Winter and Gaudet. The solid symbol drawn at y^+ = 200 for each Mach number corresponds to the error in a measured profile due to a 4 % error in c_f (i.e. a 2 % error in u_τ). As will be seen the differences between the two laws could easily be masked in any experimental comparison by possible errors in skin-friction.

Appendix B

Relationship between p_{rT} and p_{rt}

By definition $p_{rT} = \frac{\nu_t}{k_T}$ and $p_{rt} = \frac{\nu_t}{\kappa_t}$

where $k_T = - \overline{\rho v' H'} / \rho \frac{\partial H}{\partial y}$

$\kappa_t = - \overline{\rho v' h'} / \rho \frac{\partial h}{\partial y}$

and $\nu_t = - \overline{\rho v' u'} / \rho \frac{\partial u}{\partial y}$

Assuming that $v < u$ and $(u'^2 + v'^2 + w'^2) \ll u^2$, it follows that

$H' = h' + u u'$. Also $\frac{\partial H}{\partial y} = \frac{\partial h}{\partial y} + u \frac{\partial u}{\partial y}$.

Thus $\frac{p_{rt}}{p_{rT}} = \frac{(\overline{\rho v' h'} + u \overline{\rho v' u'}) \frac{\partial h}{\partial y}}{\overline{\rho v' h'} \frac{\partial H}{\partial y}}$

$= 1 + \frac{(p_{rt} - 1) u_1^2 \bar{u} \frac{\partial \bar{u}}{\partial y}}{\frac{\partial H}{\partial y}}$

where $\bar{u} = u/u_1$.

With high heat transfer rates $(H_w \ll H_o)$,

$H \doteq H_w + (H_o - H_w) \bar{u}$

$\therefore \frac{p_{rt}}{p_{rT}} = 1 + \frac{(p_{rt} - 1) u_1^2 \bar{u} \frac{\partial u}{\partial y}}{(H_o - H_w) \frac{\partial u}{\partial y}}$

$= 1 + \frac{(p_{rt} - 1) \frac{u_1^2}{2H_o} \cdot 2u}{1 - \frac{H_w}{H_o}}$

For perfect gas $\frac{H_w}{H_o} = \frac{T_w}{T_{ol}}$ and $\frac{u_1^2}{2H_o} = \frac{\frac{\gamma - 1}{2} M_1^2}{1 + \frac{\gamma-1}{2} M_1^2}$

From (4) we see that $p_{rt} = p_{rT}$ at the wall $\bar{u} = 0$. Away from the wall p_{rT} is only equal to p_{rt} if $p_{rt} = 1$. For $p_{rt} < 1$, p_{rT} is greater than p_{rt} reaching a maximum value in the free stream. Typical values are plotted in Figure 30 where it will seem that as the wall temperature rises the variation of p_{rT} through the layer increase rapidly, for example with $T_w/T_{ol} = 0.6$ at $M = 6$, p_{rT} reaches 7 at the edge of the layer.

At adiabatic conditions the total enthalpy distribution can be approximated by $H = H_r + (H_o - H_r)\bar{u}^2$.

Thus $\frac{p_{rt}}{p_{rT}} = 1 + \frac{p_{rt} - 1}{1 - r}$

where r is the recovery factor. For $p_{rt} = 0.9$ and $r = 0.9$ this shows that $p_{rT} \rightarrow \infty$. In fact over the inner part of the layer H increases rather more rapidly than is implied by $(H_o - H_r)u^2$ (see Figure 9) so that p_{rT} does not in fact, tend to infinity. It is however, very large and thus any calculations with $p_{rT} = 1$ are likely to be in error near adiabatic conditions.

Notation

A_o, A	Damping lengths
B	Additive constant in law of the wall
c_o	Constant in eddy viscosity
c_f	Skin friction
c_p	Specific heat at constant pressure
E_s	Reference Eckert No
H	Total enthalpy
h	Static enthalpy
k	Thermal conductivity (laminar)
k_t	Thermal conductivity (turbulent)
M	Mach number
p	Pressure
p^+	Non-dimensional pressure gradient
p_r	Laminar Prandtl number
p_{rt}	Turbulent Prandtl number based on static enthalpy
p_{rT}	Turbulent Prandtl number based on total enthalpy
q	Heat flux
r	Recovery factor
S_t	Stanton Number
T	Static temperature
T_o	Total temperature
u	Streamwise velocity
$\bar{u}$	u/u_1
u_τ	Frictional velocity
u_τ^i	Transformed frictional velocity (Section 3.1.2)
u^+	u/u_τ
u^x	Van Driest transformed velocity (eqn (13))
u^{xx}	Transformed velocity with injection (eqn (35))
v	Normal velocity
v_w	Normal injection velocity
v^+	v_w/u_τ
κ	Von Karman constant
ρ	density
μ	viscosity

ν	Kinematic viscosity
ν_t	Turbulent eddy voscosity
γ	Ratio of specific heat capacities
θ	Momentum thickness
δ	Boundary layer thickness
δ^x	Displacement thickness
δ^x_k	Kinematic displacement thickness

Suffices

w	Wall
1	Free stream
t	Turbulent
r	Recovery conditions

Author		M	Rθ	Cf	Cf corrected
Mabey		2·493	14700	·00162	·00162
		2·470	6300	·00180	·00179
		2·482	11200	·00160	·00159
		2·500	17000	·00156	·00156
		2·544	21600	·00152	·00154
		2·525	19000	·00155	·00156
		2·522	14900	·00160	·00161
		2·496	9100	·00167	·00167
		2·495	7400	·00172	·00172
		2·493	5700	·00185	·00185
		2·497	13300	·00156	·00156
		2·490	11100	·00164	·00164
		2·492	8600	·00172	·00172
		2·425	26400	·00138	·00135
		2·417	21300	·00141	·00141
		2·411	11900	·00145	·00142
Winter		2·402	39,500	·00135	·00132
		2·600	40,500	·00129	·00132
Coles		2·540	2190	·00242	·00244
		2·568	6600	·00181	·00184
		2·578	10200	·00166	·00169
Schutts		2·502	6080	·00180	·00180
		2·533	9640	·00158	·00159
		2·451	18800	·00156	·00154

Table 1. Corrected skin-friction coefficients used in Figure 8.

References

1	Verma, V.K.	A method of calculation for two-dimensional and axisymmetric boundary layer. Cambridge University Engineering Department Report CUED/A_Aero/TR3 1971.
2	Cebeci T and Smith A.M.O.	A finite-difference method for calculating compressible laminor and turbulent boundary layers. Jour. of Basic Engineering. Vol.92, p.523, 1970.
3	Van Driest,E.R.	Turbulent boundary layers in Compressible flow. Jour. Aero. Sci. Vol.18, p.145, 1951.
4	Fenter,W.F. Stalmach,C.J.	The measurement of turbulent boundary layers shear stress by means of surface impact-pressure probes. Jour. Aero/Space Sci. Vol.25, p,793, 1958.
5	Mabey.D.G. Meier.H.U. Sawyer.W.G.	Experimental and theoretical studies of the boundary layer on a flat plate at Mach numbers from 2•5 to 4•5. R.A.E. Report to be issued. Also paper 2 in AGARD Conf. Proc 93, 1971.
6	Bushnell,D.M. Beckwith,I.E.	Calculation of non-equilibrium hypersonic turbulent boundary layers and comparison with experimental data. A.I.A.A. Jour. Vol.8, p,1462. 1970.
7	Fernholz,H.	Departures from a fully developed turbulent velocity profile on a flat plate in compressible boundary layers. In Fluid Dynamic Transactions, Vol.5, Polish Scientific Publishers, Warsaw. 1972.
8	Danberg.J.E.	Characteristics of the turbulent boundary layer with heat and mass transfer at M = 6•7 N.O.L.T.R. 64-99, 1964.
9	Hopkins.E.J. Keener.E.R. Polek.T.E. Dwyer.H.A.	Hypersonic turbulent skin-friction and boundary-layer profiles on non-adiabatic flat plates. A.I.A.A. Jour. Vol.10. pp.40-48, 1972.
10	Winter.K.G. Gaudet.	Turbulent boundary-layer studies at high Reynolds numbers at Mach numbers between 0•2 and 2•8. ARC R & M 3712. 1970.
11	Maise.G. McDonald.H.	Mixing length and kinematic eddy viscosity in a compressible boundary layer. A.I.A.A. Jour. Vol,6, p.73. 1968.
12	Squire,L.C.	Eddy viscosity distributions in compressible turbulent boundary layers with injection. Aero Quart Vol. XX111. p.169. 1971.

References

13 Cebeci,T.
Smith,A.M.O.
Mosinskis,G.
Calculations of compressible, adiabatic turbulent boundary layers.
AIAA. Jour. Vol.8, p.1973, 1970.

14 Keener,E.R.
Polek,T.E.
Measurements of Reynolds analogy for hypersonic turbulent boundary layers on a non-adiabatic flat plate.
AIAA. Jour. Vol.10, p 845, 1972.

15 McQuaid,J.
Experiments on incompressible turbulent boundary layers with distributed injection,
ARC R & M No.3549. 1967.

16 Simpson,R.L.
Moffat,R.T.
Kays,W.M.
The turbulent boundary layer on a porous plate; experimental skin-friction with variable injection and suction.
Int. Jour. Heat Mass Transfer, Vol.12, p,771,1969.

17 Kendall,R.M.
Rubesin,M.W.
Dahm,T.J.
Mendenhall,M.R.
Mass, momemtum and heat transfer within a turbulent boundary layer with foreign gas mass transfer at the surface. Part I, constant fluid properties
Vidya report 111, 1964.

18 Baker.R.J.
Jonsson,V.K.
Launder,B.E.
The turbulent boundary layer with streamwise pressure gradient and foreign-gas injection.
Imperial College, Dept. of Mechanical Engineering.
Report No. EHT/TN/G/31, 1971.

19 Anderson,P.S.
Kays,W.M.
Moffat,R.J.
The turbulent boundary layer on a porous plate: an experimental study of the fluid mechanics for adverse free-stream pressure gradients.
Stanford University, Report HMT-15, 1972.

20 Coles,D.E.
Measurements in the boundary layer on a smooth flat plate in supersonic flow,I, the problem of the turbulant boundary layer.
Z angew: Math. Phys. Vol,5. p,181, 1954.

21 Coles,D.E.
The turbulent boundary layer in a compressible fluid.
The Rand Corporation. Report R-403-PR, 1962.

References

22 Squire,L.C. — The constant property turbulant boundary layer with injection: a re-analysis of some experimental results. Int Jour. Heat and Mass Transfer. Vol.13 p,939 1970.

23 Coles,D.E. — A survey of data for turbulent boundary layers with Mass Transfer. Paper 25 in AGARD Conf. Proc.93, 1972.

24 Mickley,H.S. Davis,R.S. — Momentum transfer for flow over a flat plate with blowing. NACA TN 4017, 1957.

25 Stevenson,T.N. — A law of the wall for turbulent boundary layers with suction or injection. The College of Aeronautics, Cranfield. Aero Report No 166, 1963.

26 Michel,R. Lili,T. — Couche limite turbulente avec injection a la paroi d'un meme gaz ou d'un gaz etranger. Paper 24, AGARD Conf.Proc. 93, 1972.

27 Kays W.M. — Heat transfer to the transpired turbulent boundary layer. Stanford University, Report HMT 14, 1971.

28 Squire,L.C. — A law of the wall for compressible turbulent boundary layers with air injection. J. Fluid Mech. Vol 37. p.449. 1969.

29 Squire,L.C. — Further experimental investigations of compressible turbulent boundary layers with air injection. ARC R & M 3627. 1968.

30 Jeromin,L.O.F. — An experimental investigation of the compressible turbulent boundary layer with air injection. ARC R & M 3526. 1966.

31 Danberg,J.E. — Characteristics of the turbulent boundary layer with heat and mass transfer: data tabulation. NOLTR 67 - 6 1967.

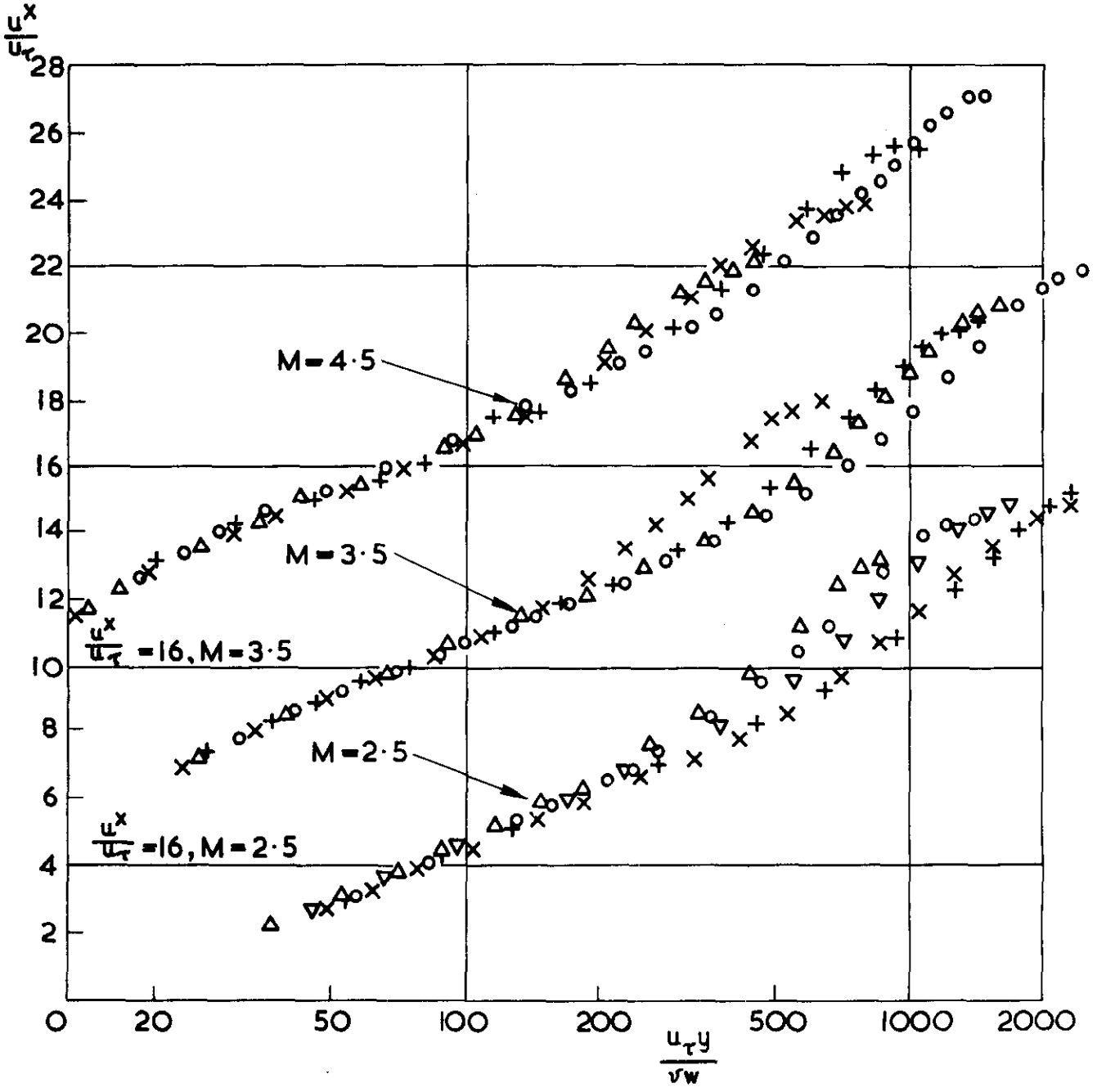

Figure 1 Law of the Wall: Experimental Results of Mabey

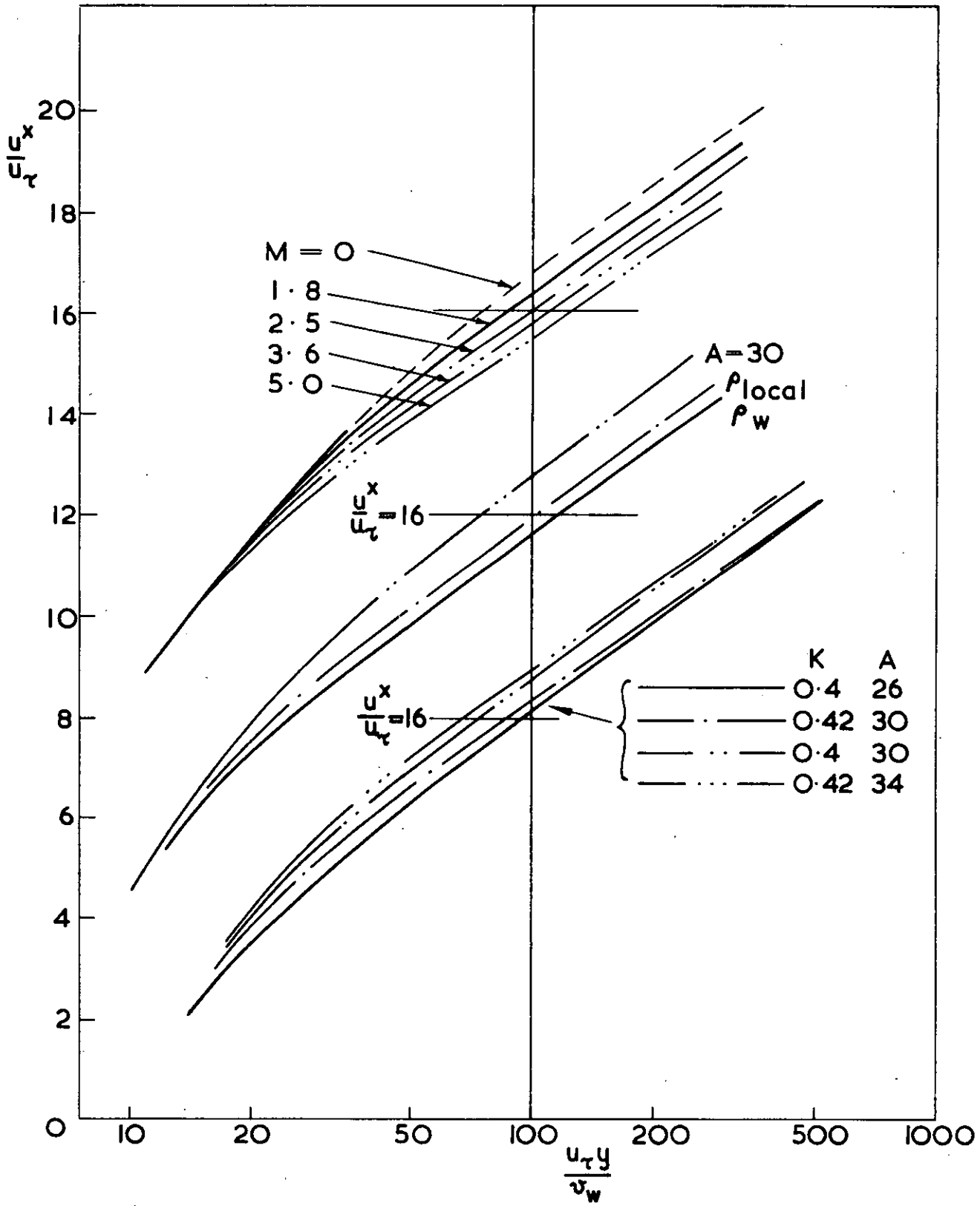

Figure 2 Calculated Law of the Wall: R_θ = 17,500

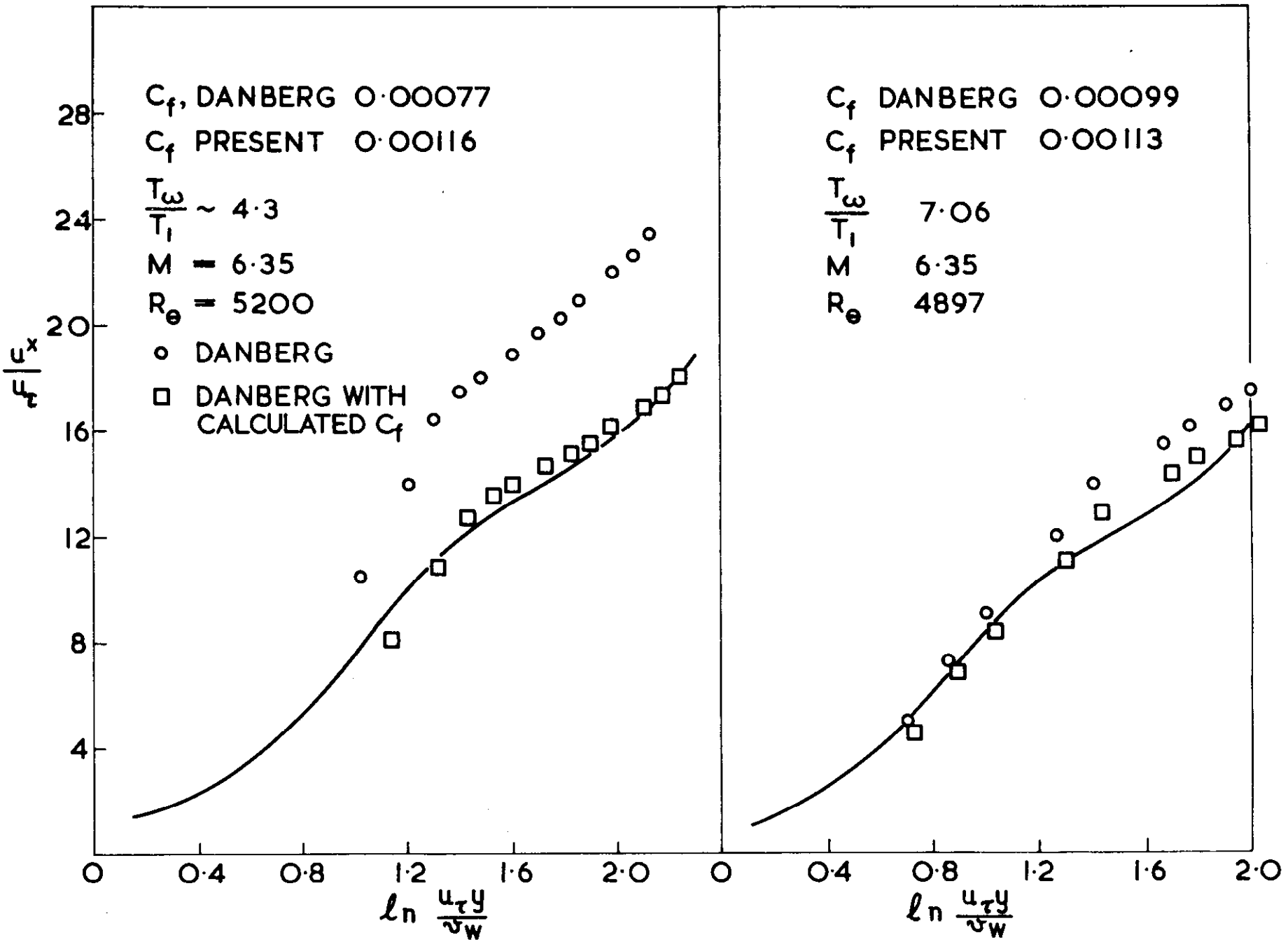

Figure 3 Law of the Wall with Heat Transfer

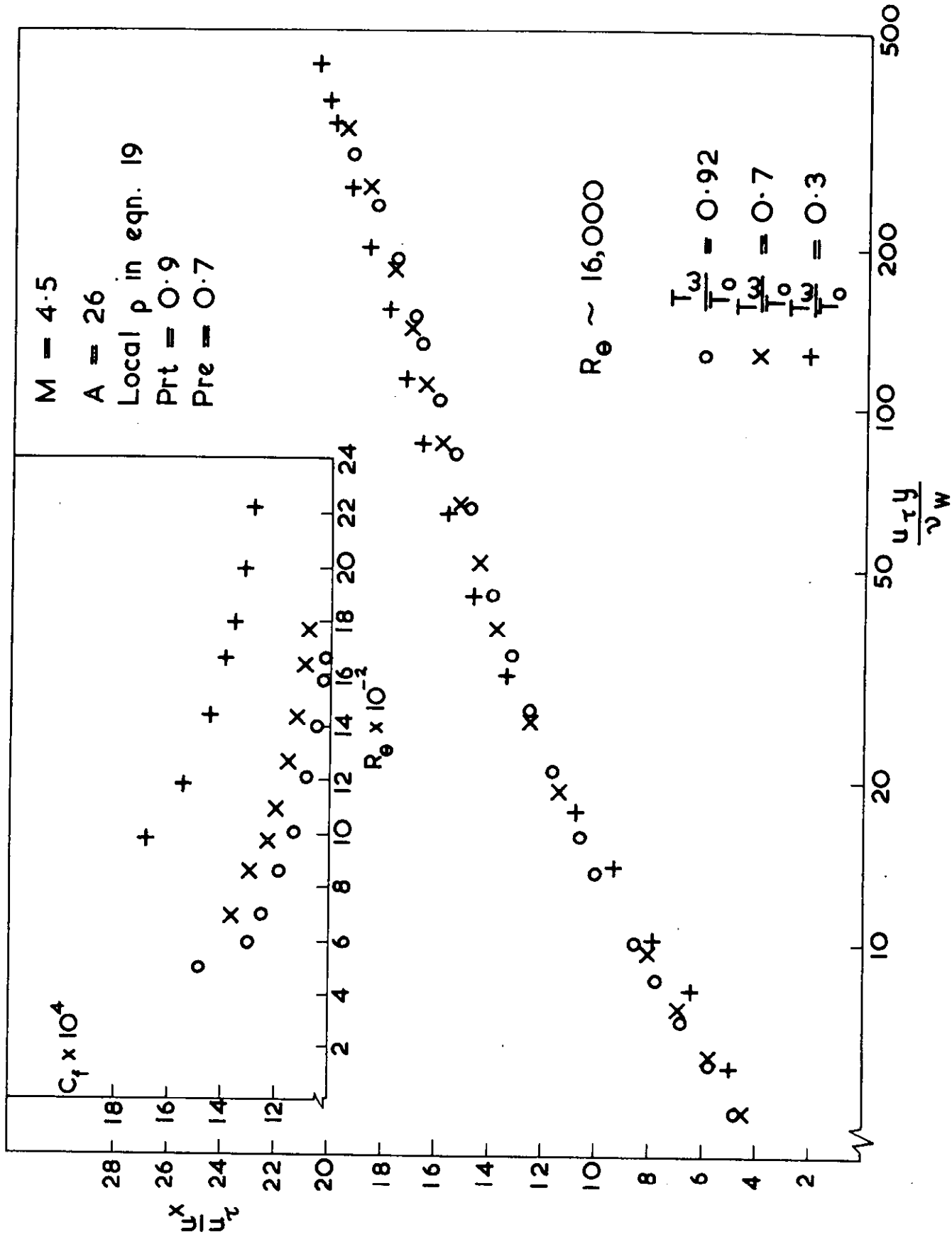

Figure 4 Effect of Heat Transfer on Law of the Wall

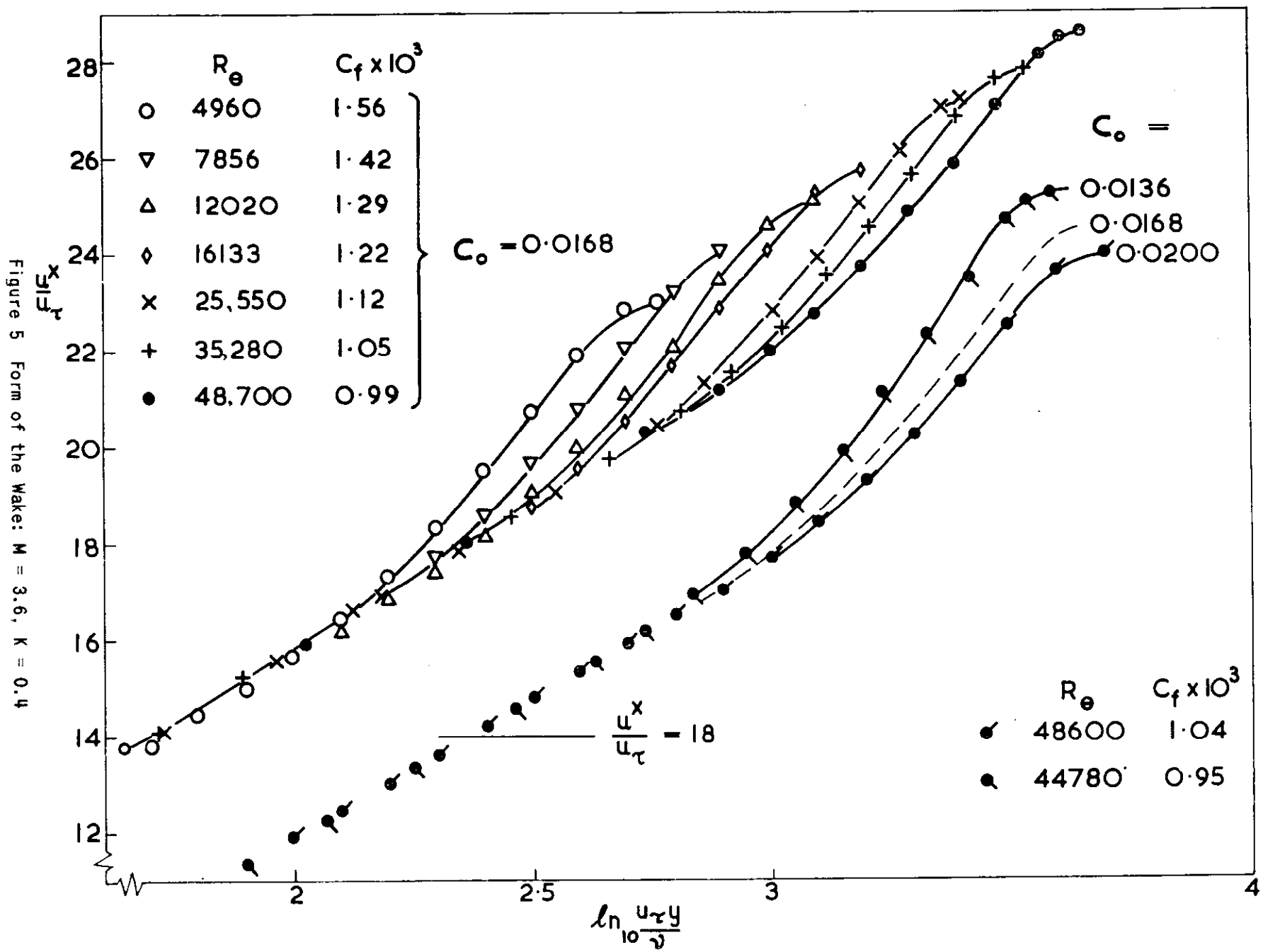

Figure 5 Form of the Wake: M = 3.6, K = 0.4

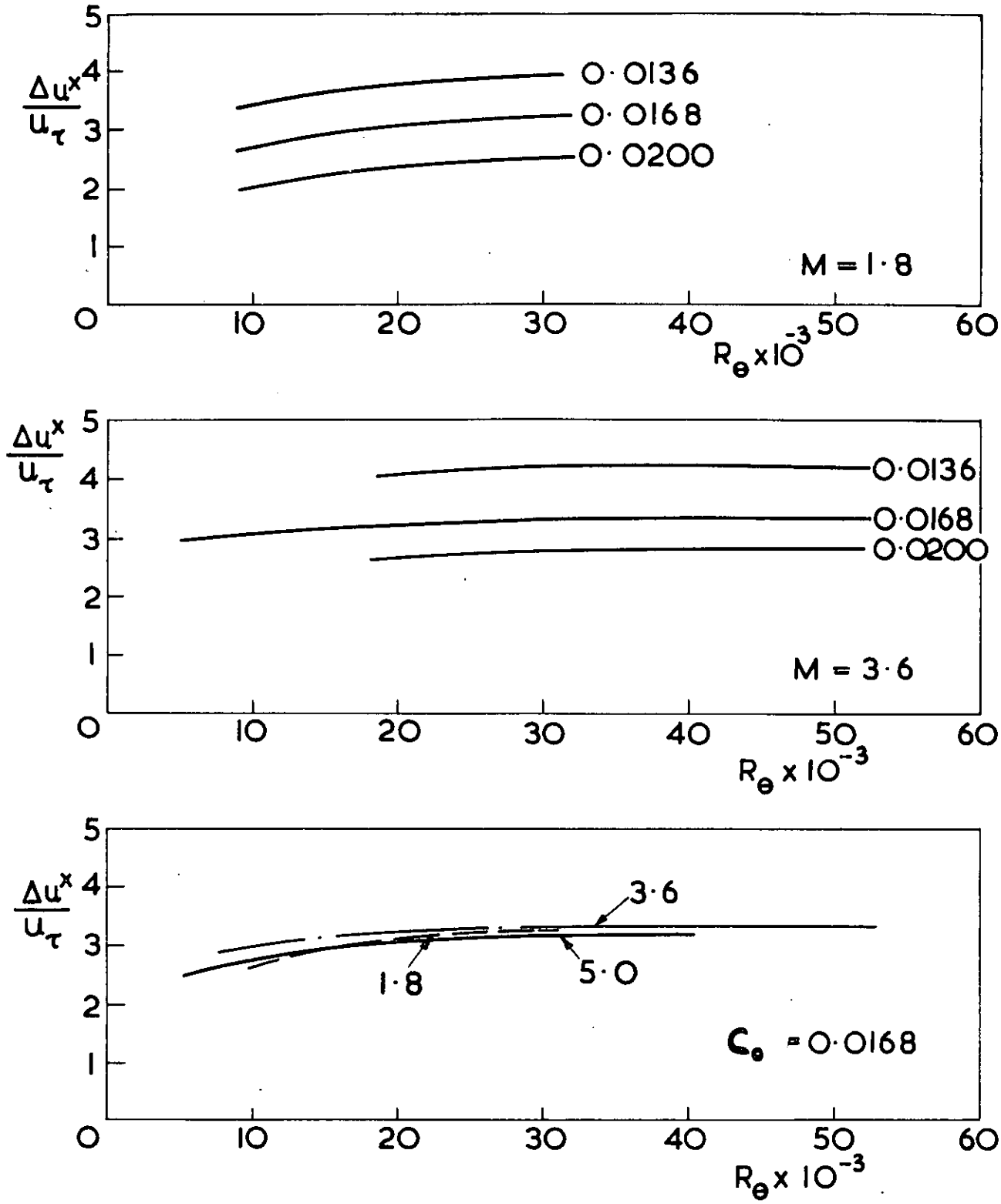

Figure 6 Summary of Wake Calculations

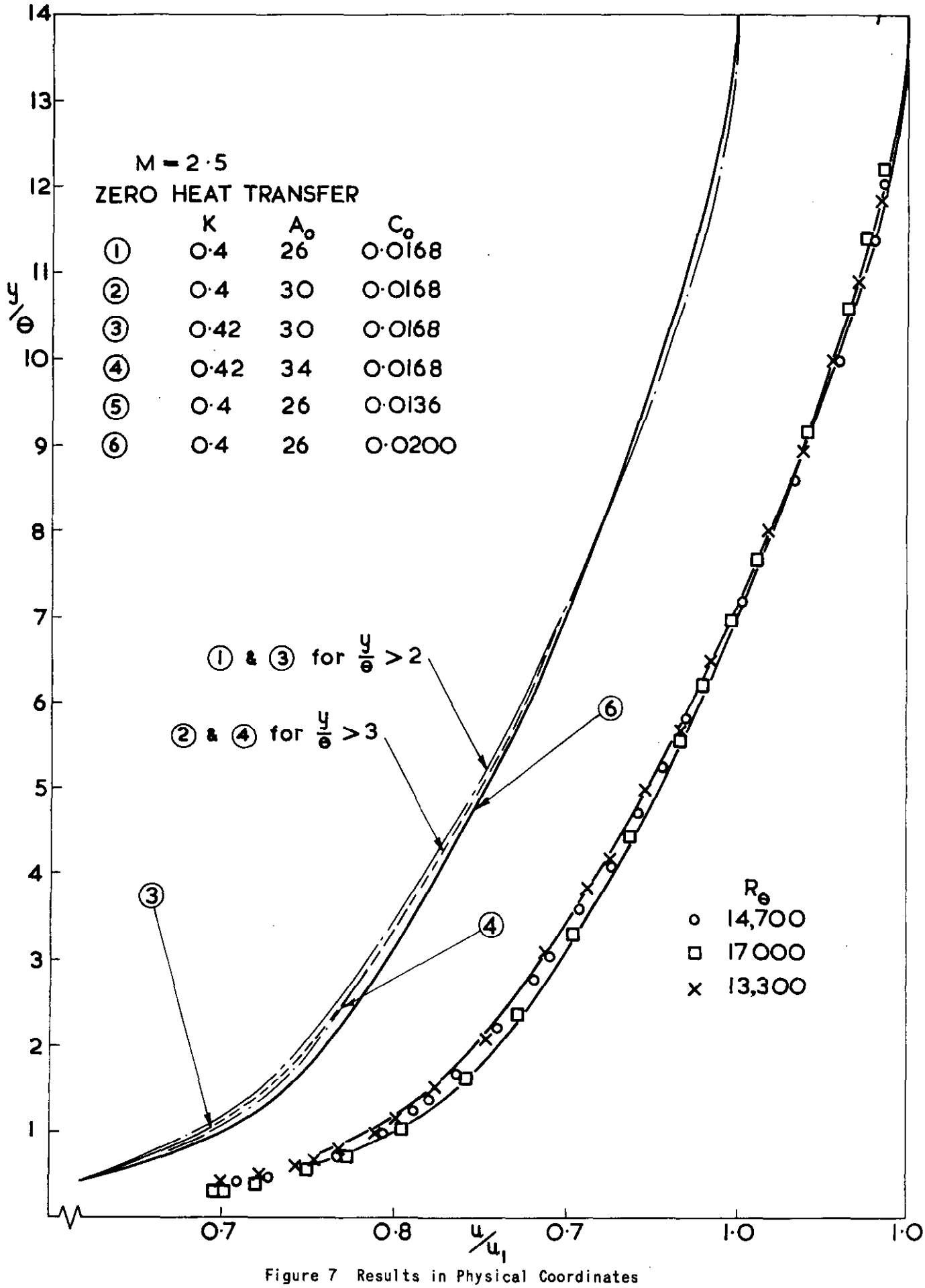

Figure 7 Results in Physical Coordinates

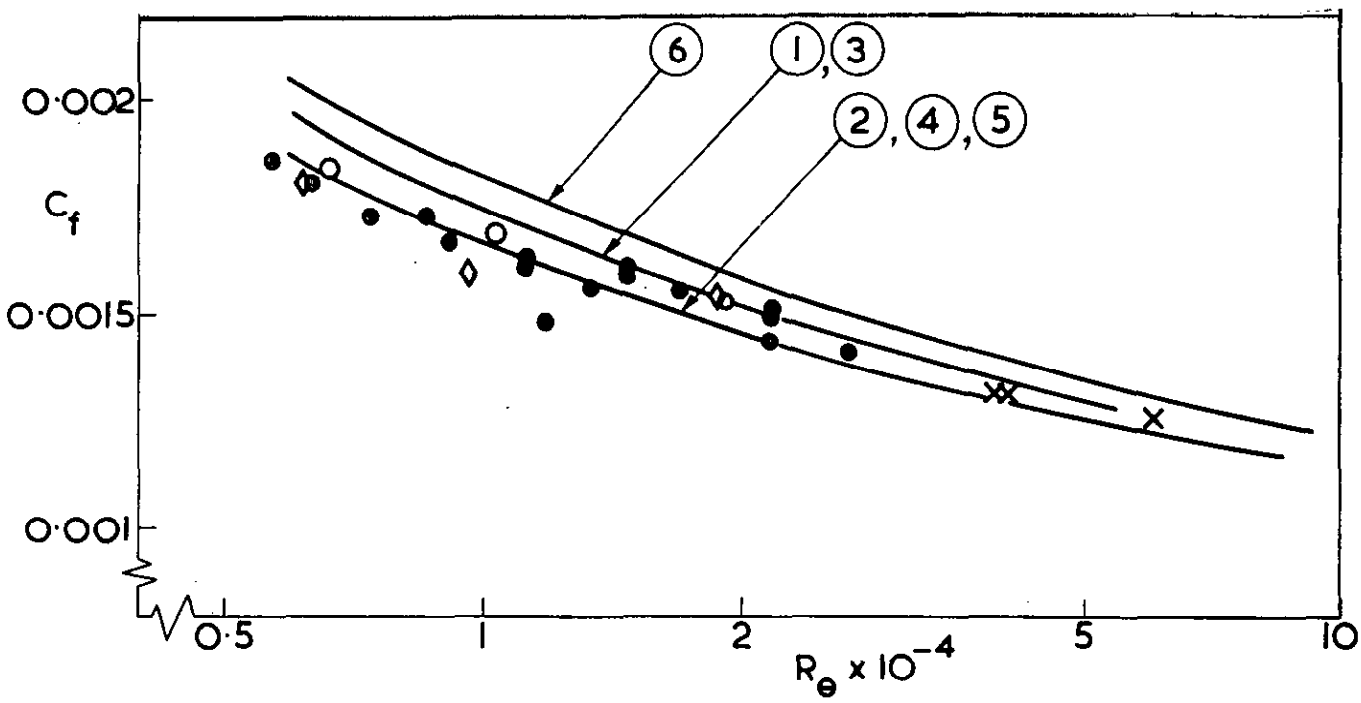

(1)	0·4	26	0·0168
(2)	0·4	30	0·0168
(3)	0·42	30	0·0168
(4)	0·42	34	0·0168
(5)	0·40	26	0·0136
(6)	0·40	26	0·0200

Measured points as in Table 1.

Figure 8 Calculated and Measured c_f : M = 2.5

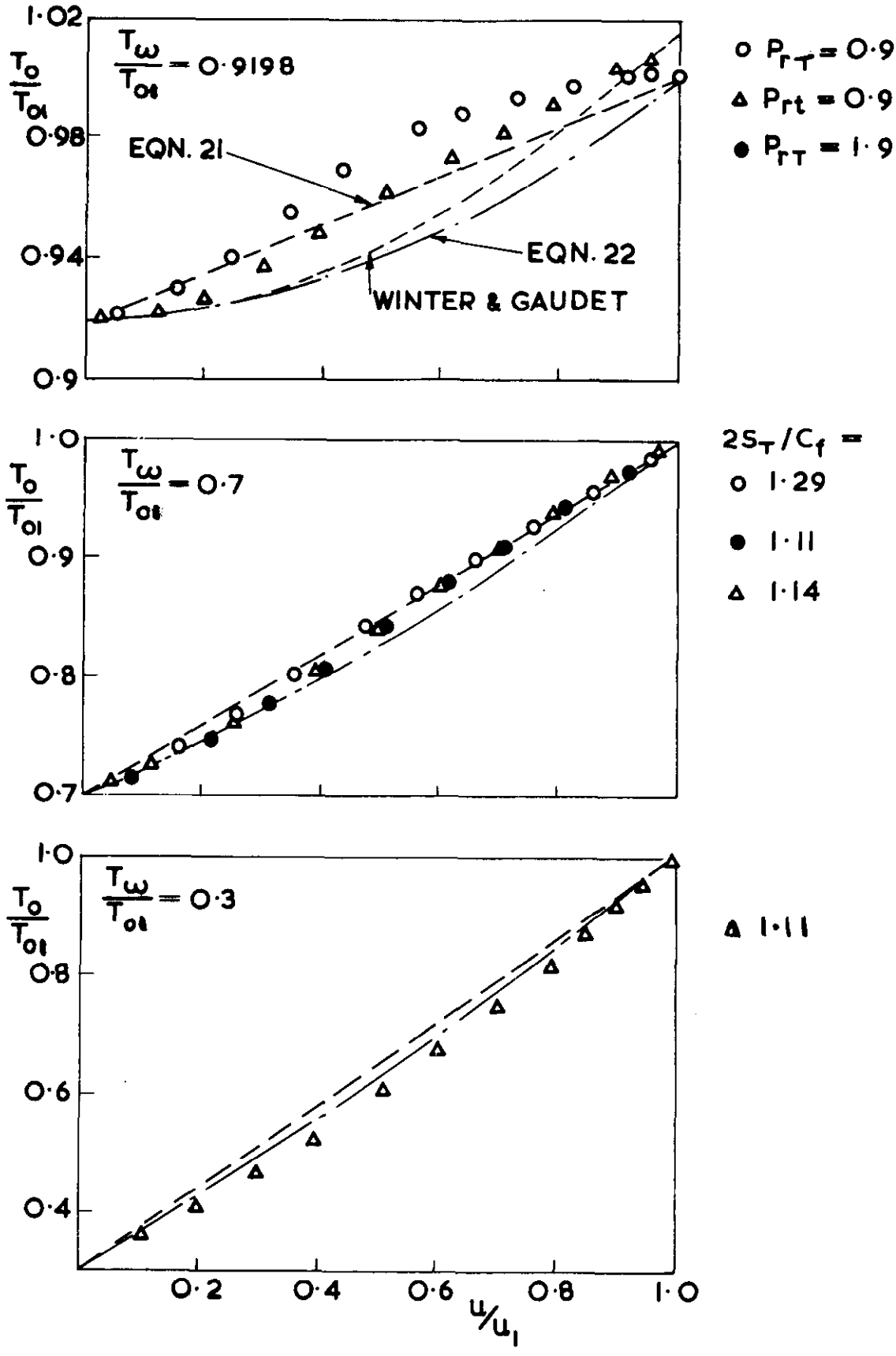

Figure 9 Calculated Total Temperature Profiles, M = 4.5

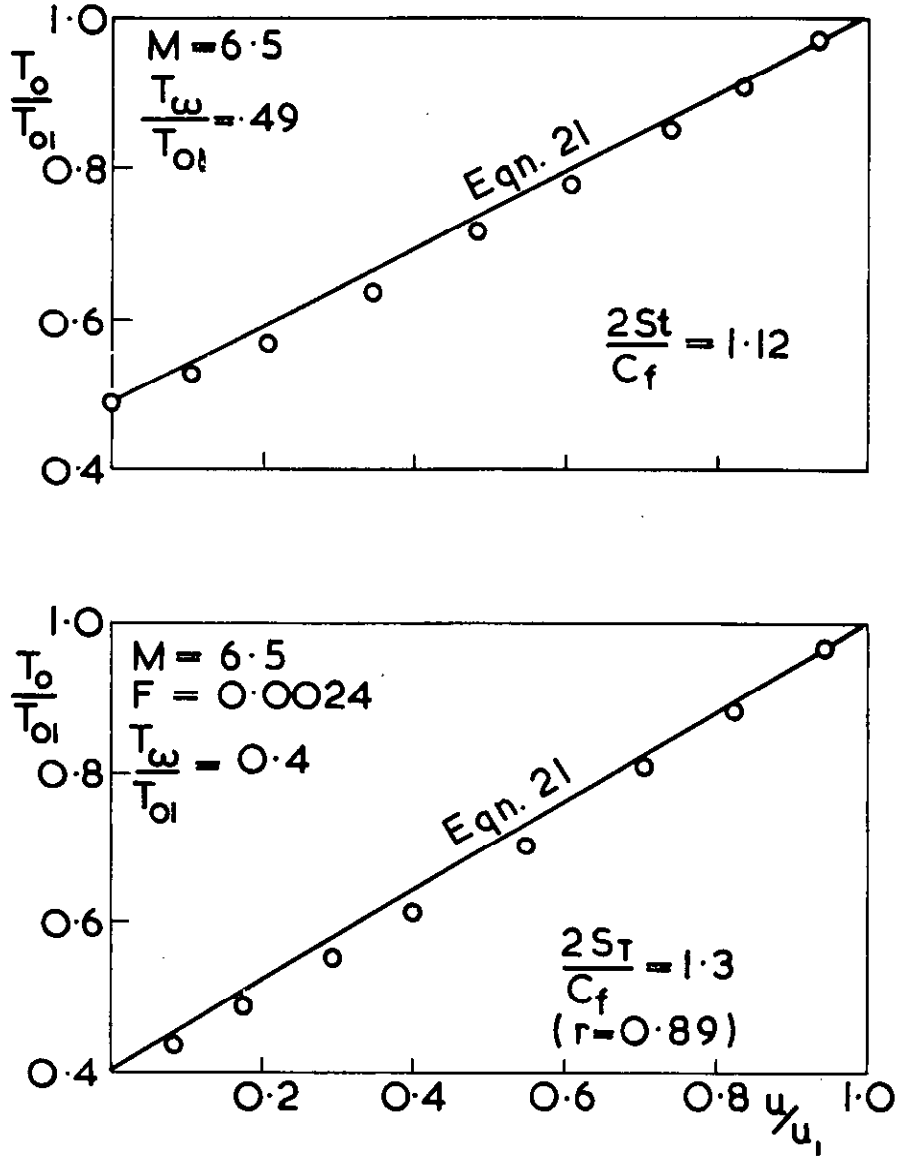

Figure 10 Calculated Total Temperature Profiles, M = 6.5

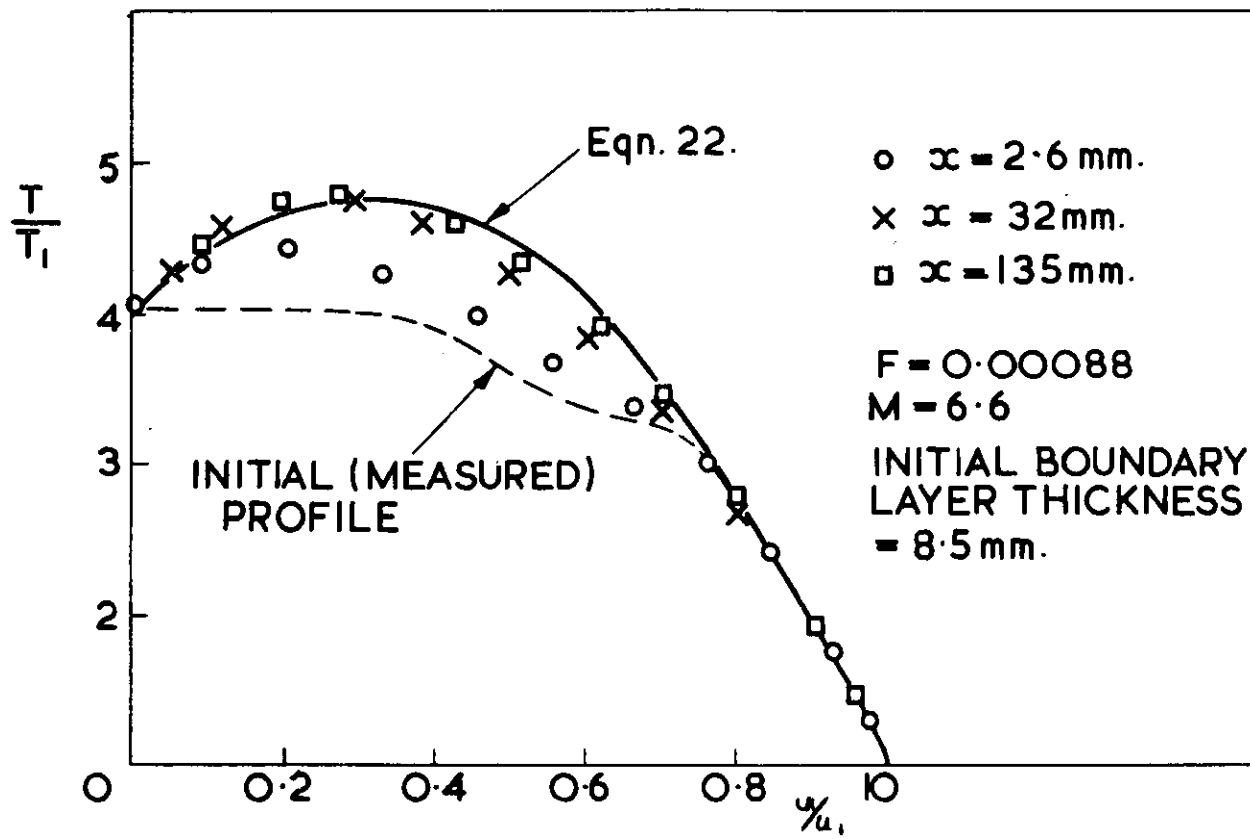

Figure 11 Development of Temperature Profiles

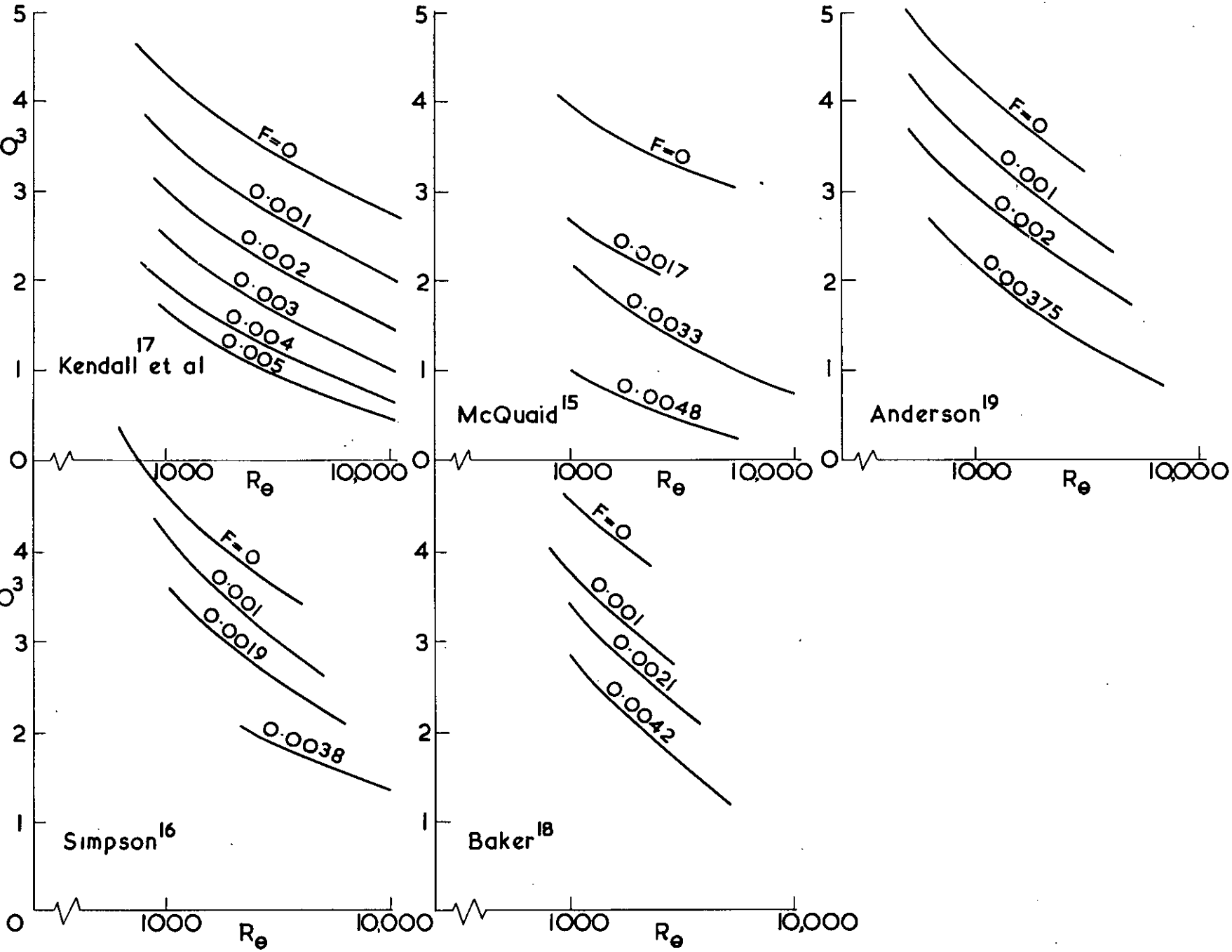

Figure 12 Experimental Results for c_f with Injection

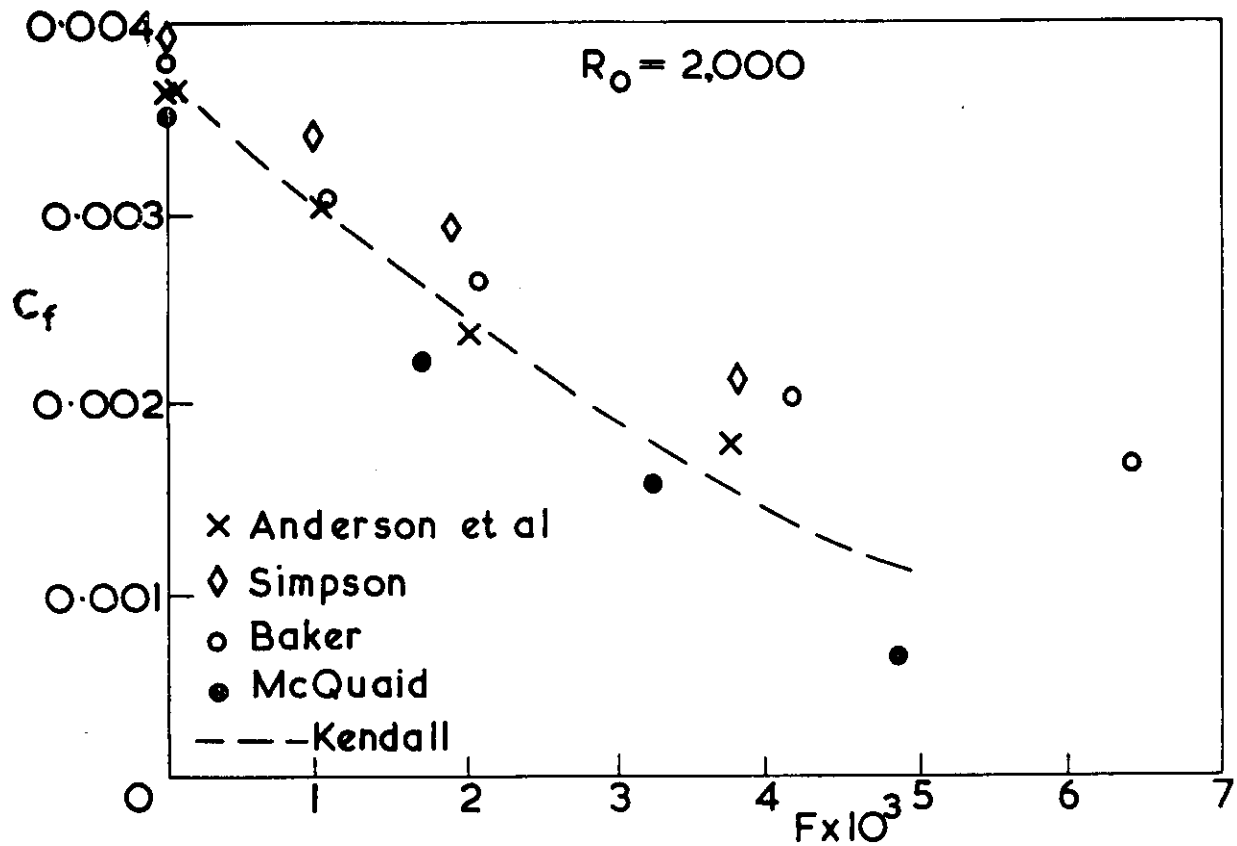

Figure 13 Experimental c_f Results: $R_\theta = 2{,}000$

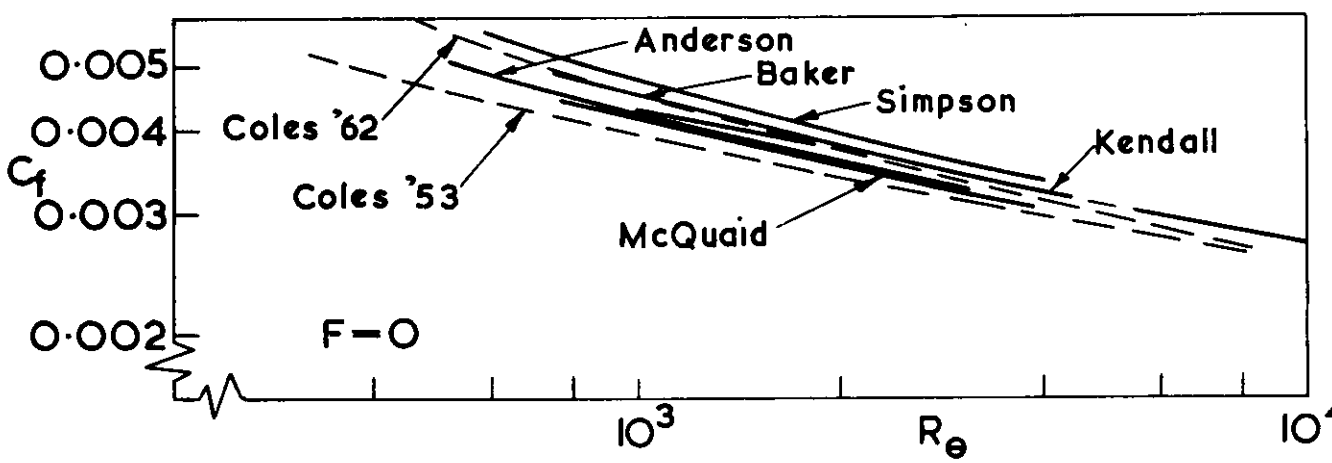

Figure 14 Experimental c_f Results: F = 0

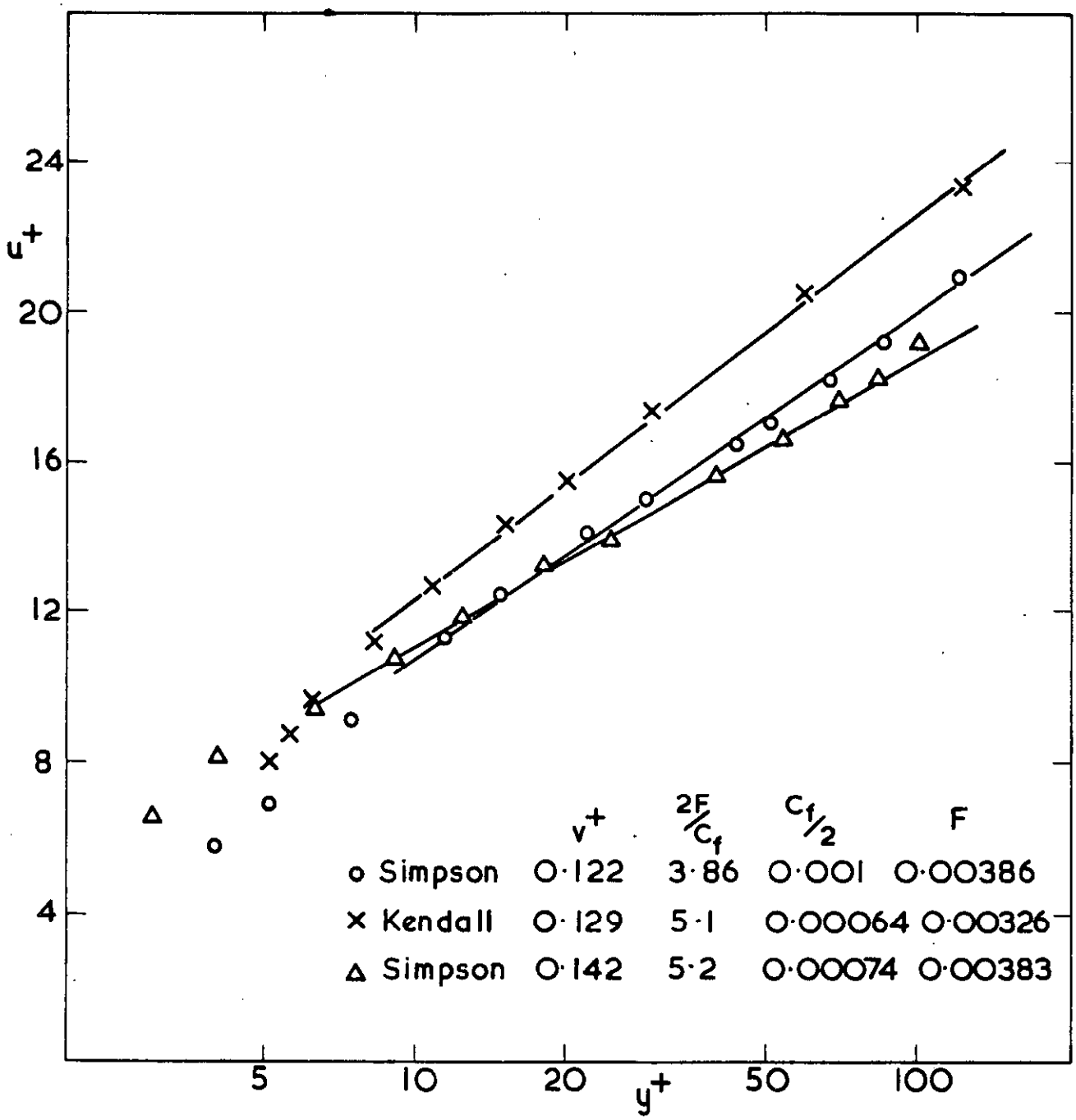

Figure 15 Variation of u^+ with y^+

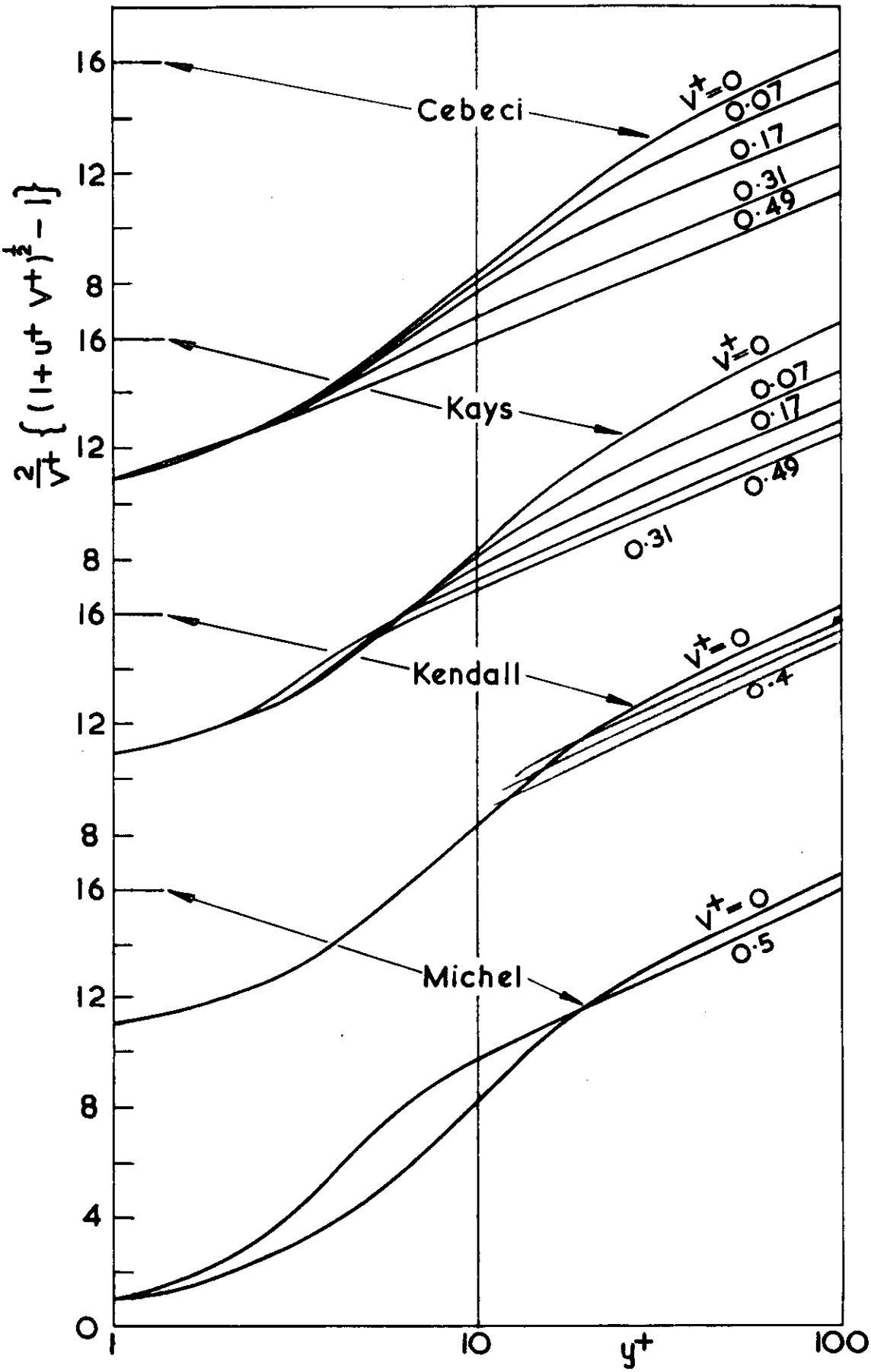

Figure 16 Law of the Wall with Injection

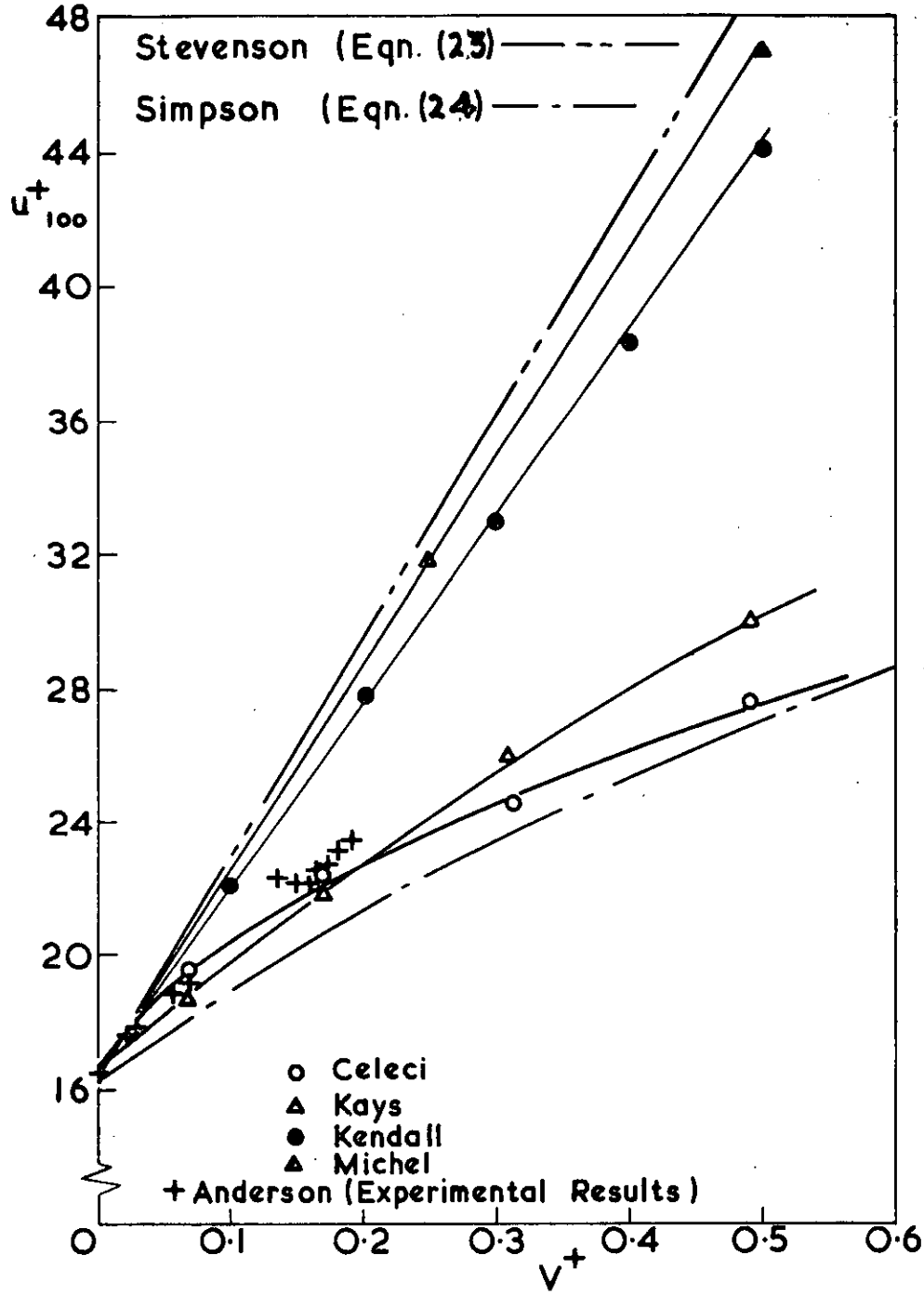

Figure 17 Variation of u^+_{100} with y^+

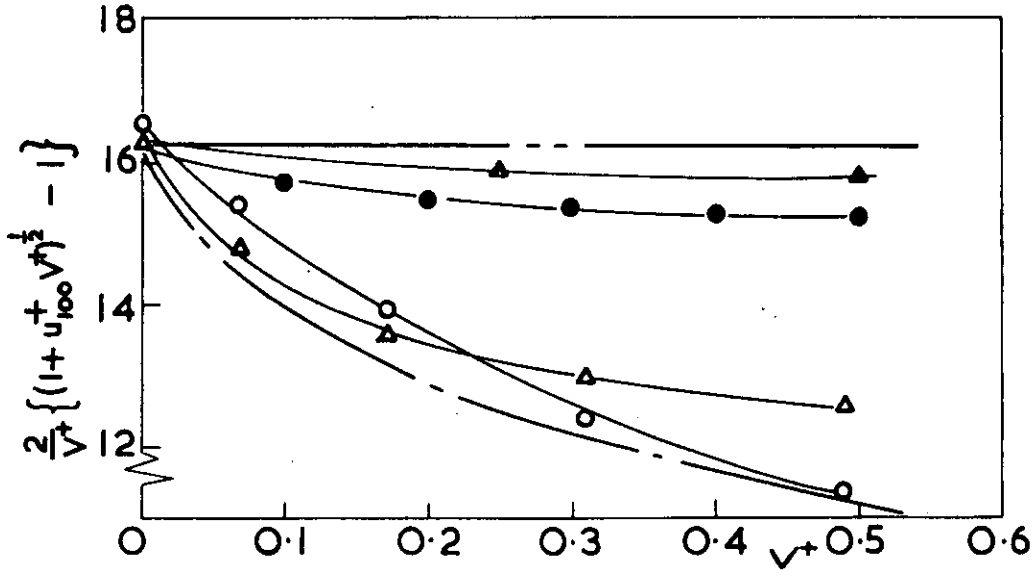

Figure 18 Variation of Stevenson's velocity at $y^+ = 100$ with v^+

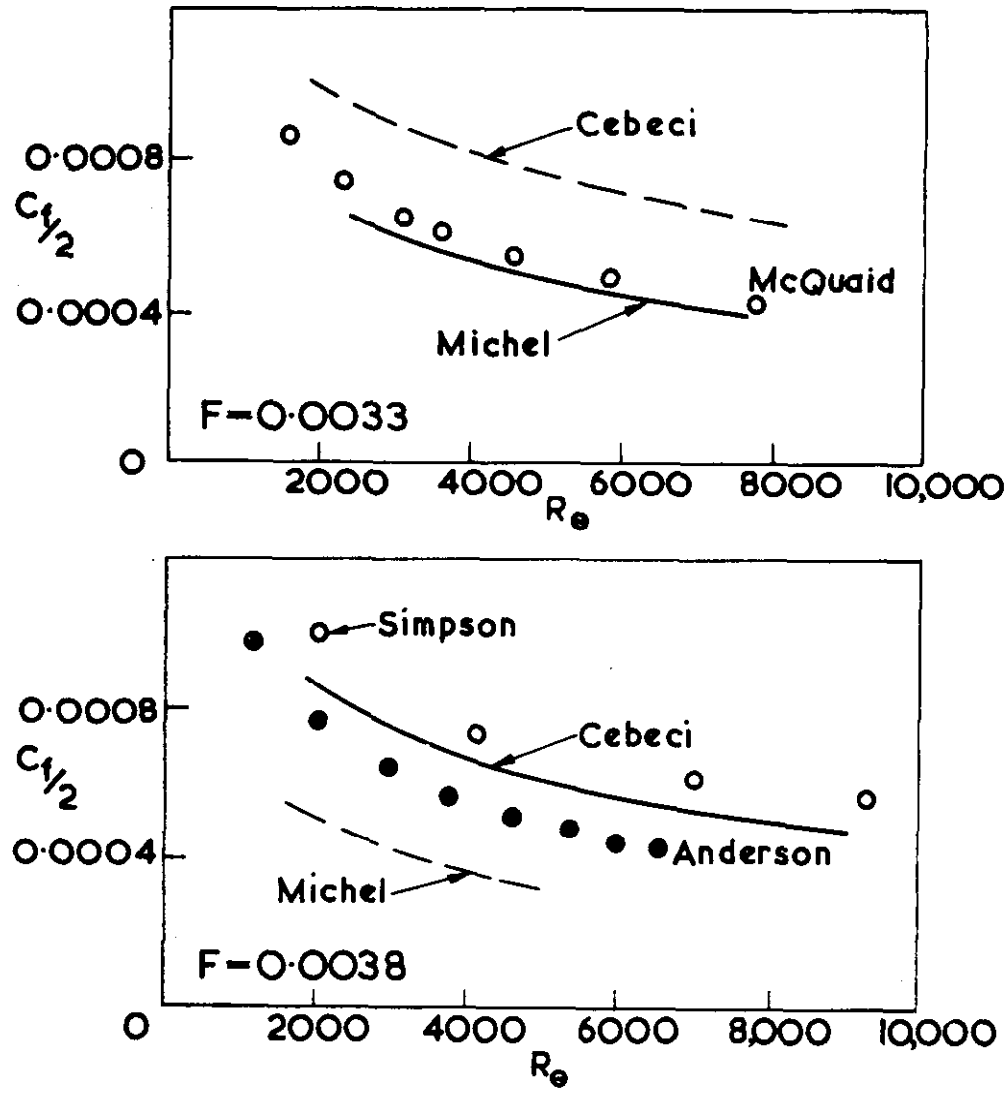

Figure 19 Calculated and Measured c_f at Low Speeds

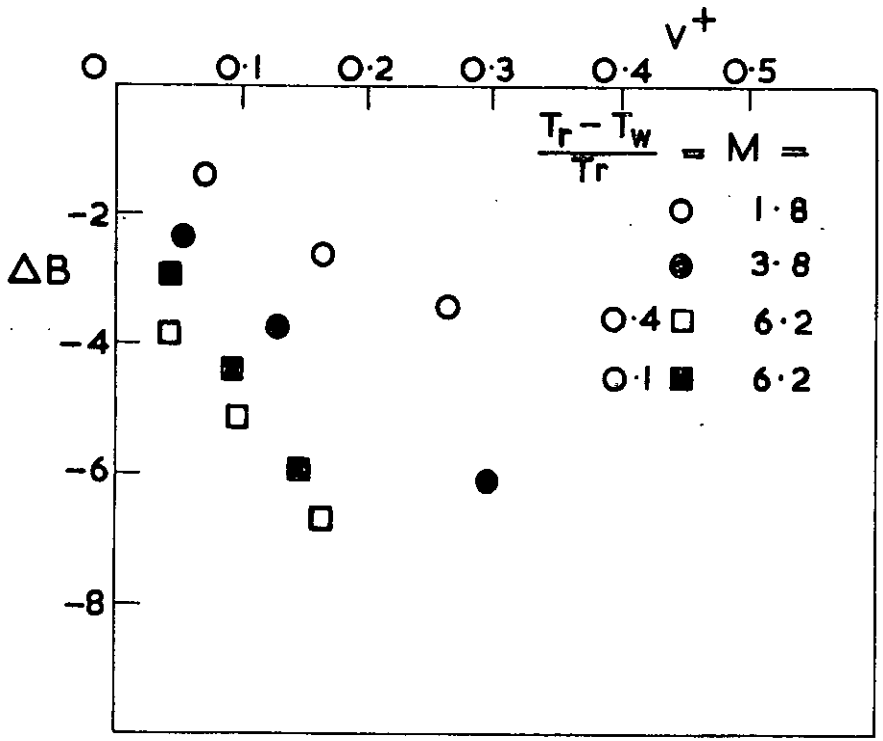

Figure 20 Variation of ΔB with v^+

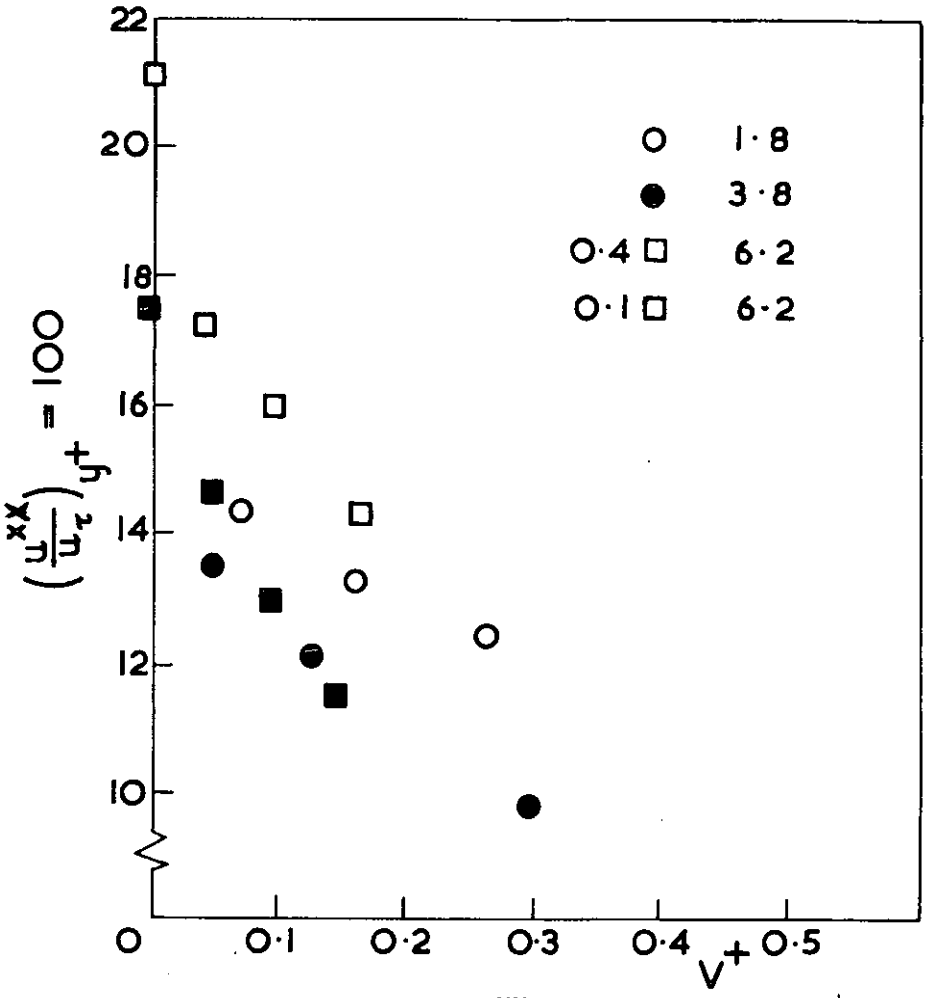

Figure 21 Variation of $(u^{xx}/u_\tau)100_\tau)100$ with v^+

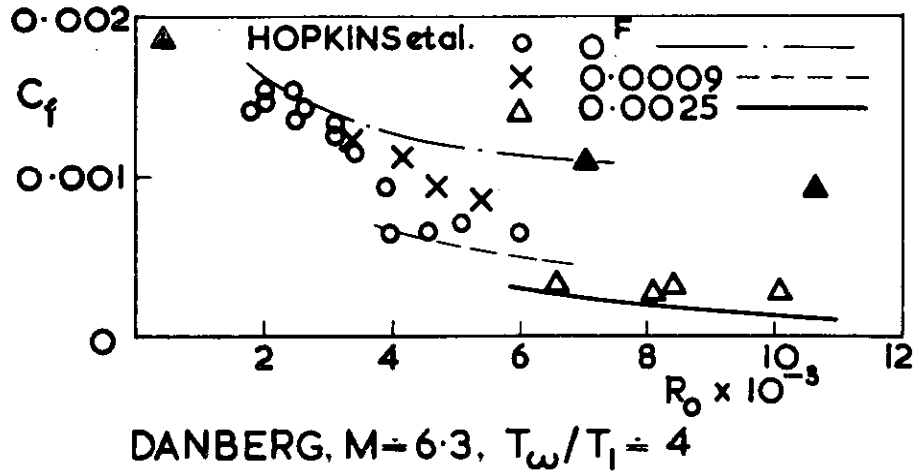

DANBERG, $M \doteq 6{\cdot}3$, $T_\omega / T_1 \doteq 4$

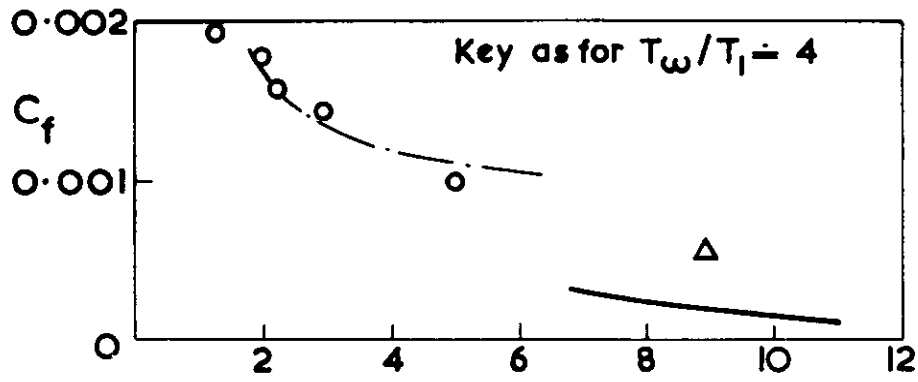

DANBERG, $M = 6{\cdot}3$ $T_\omega / T_1 \doteq 7{\cdot}5$

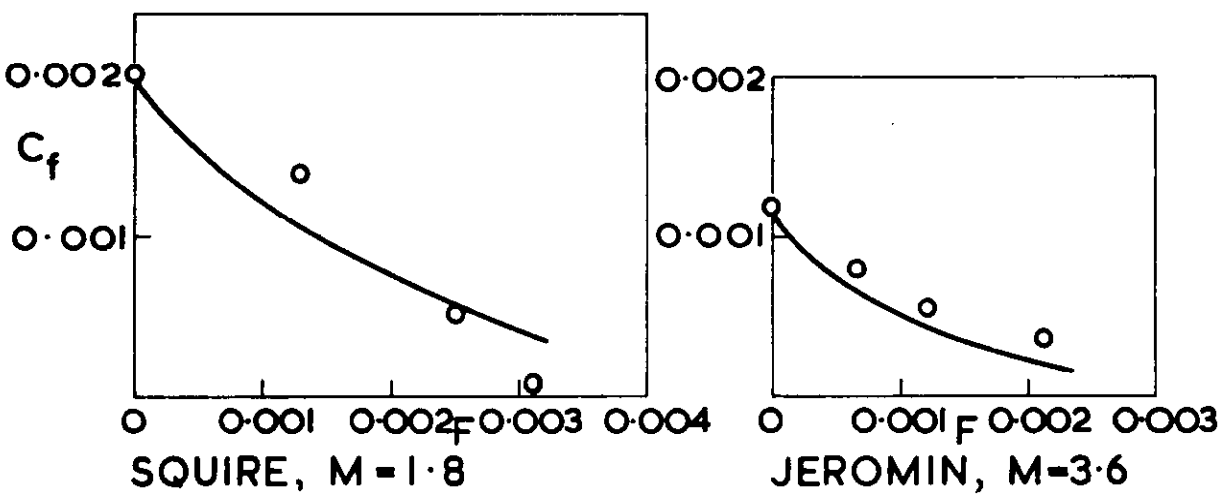

SQUIRE, $M = 1{\cdot}8$ JEROMIN, $M = 3{\cdot}6$

Figure 22 Calculated and Measured c_f with Injection

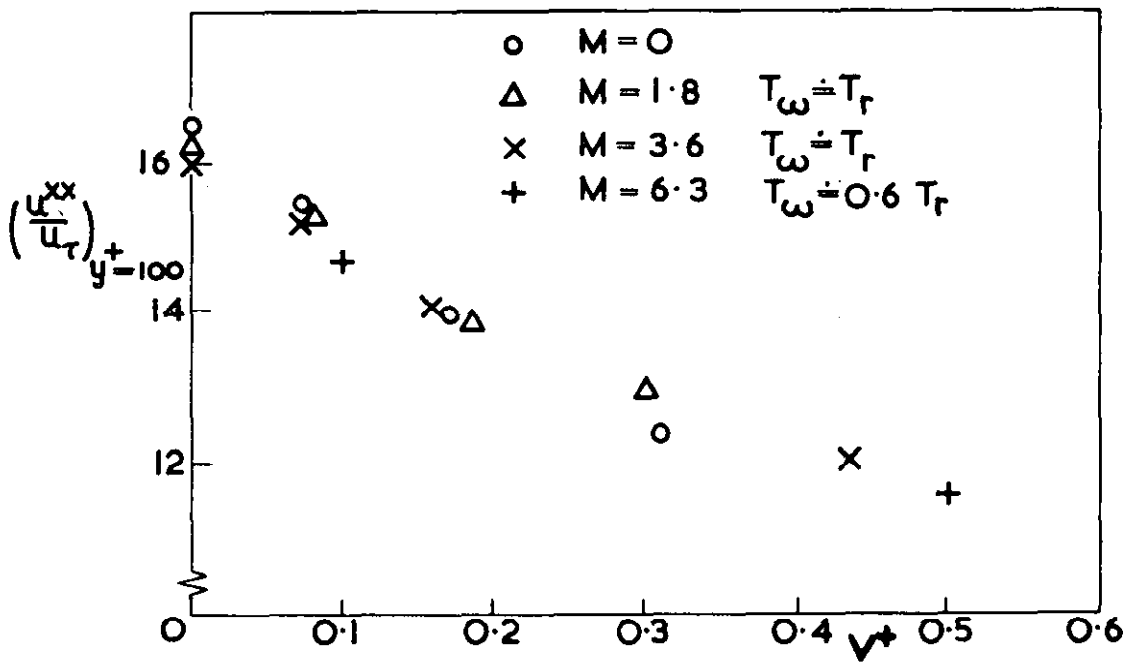

Figure 23 Variation of (u^{xx}/u_τ) at $y^+ = 100$ with v^+

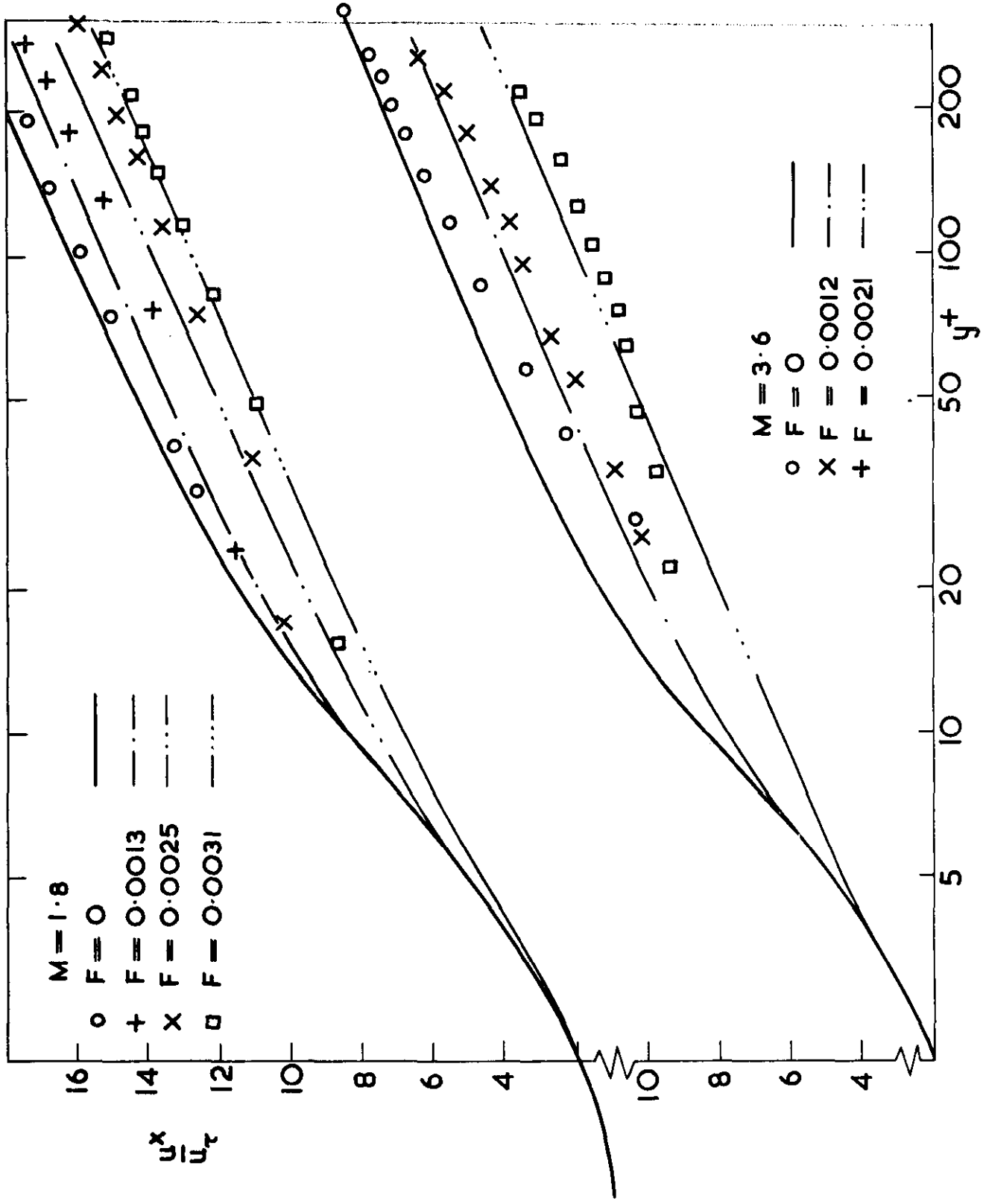

Figure 24 Calculated and Measured Profiles at M = 1.8 and 3.6: Law of the Wall Coordinates

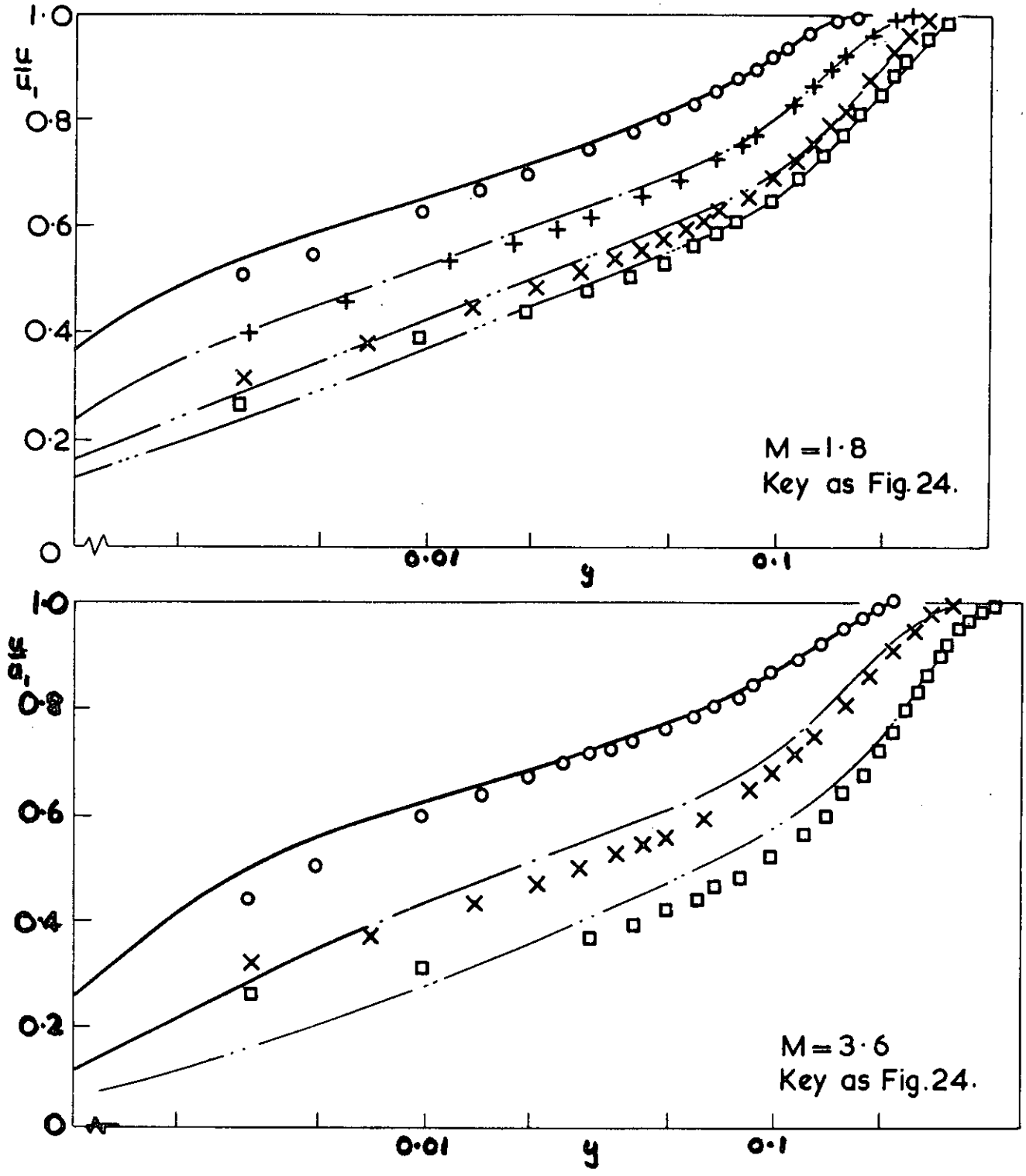

Figure 25 Calculated and Measured Profiles at M = 1.8 and 3.6: Physical Coordinates

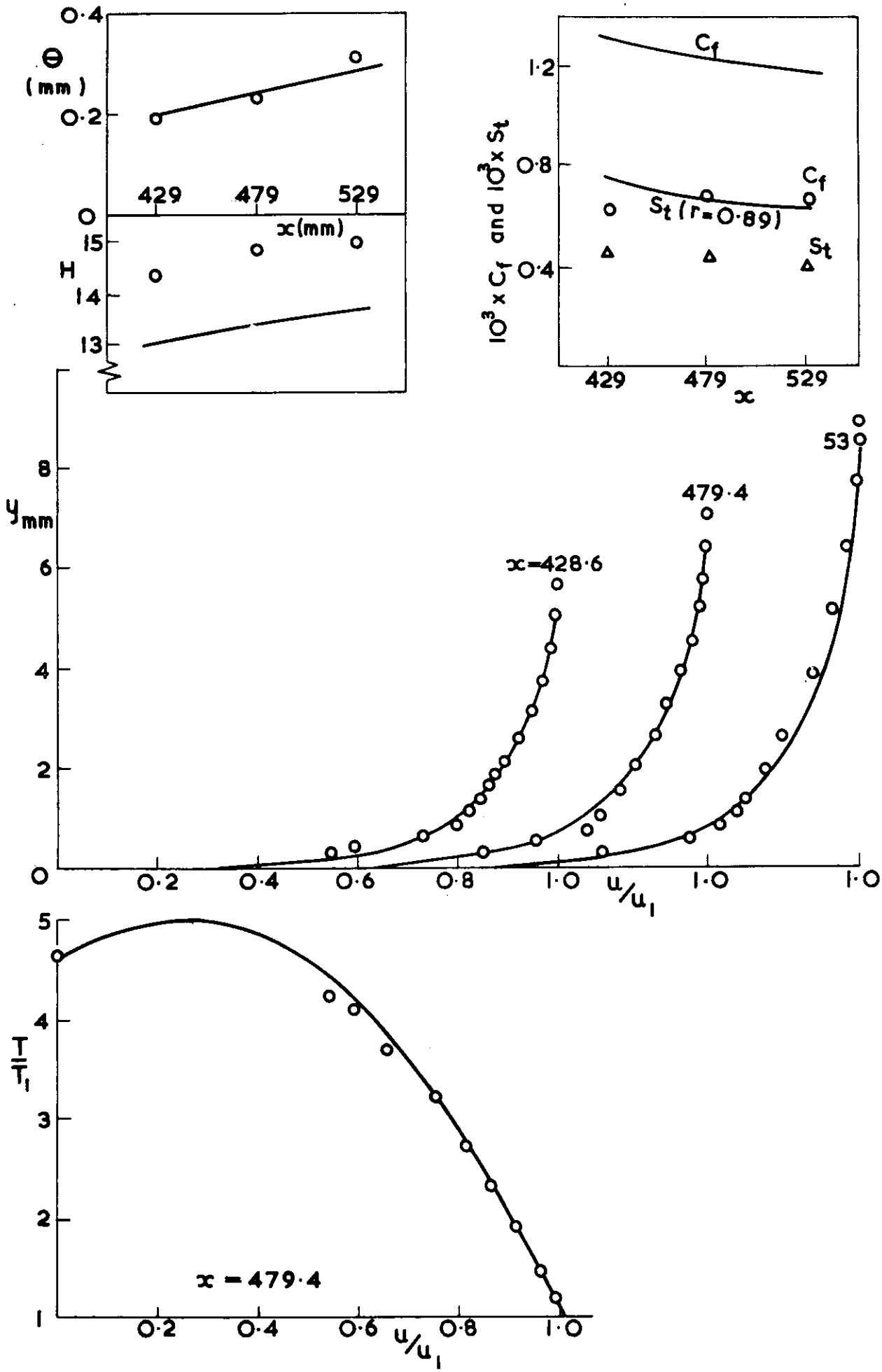

Figure 26 Results for M = 6.5, T_w/T_1 = 4.7, F = 0. Symbols for Danberg's results.

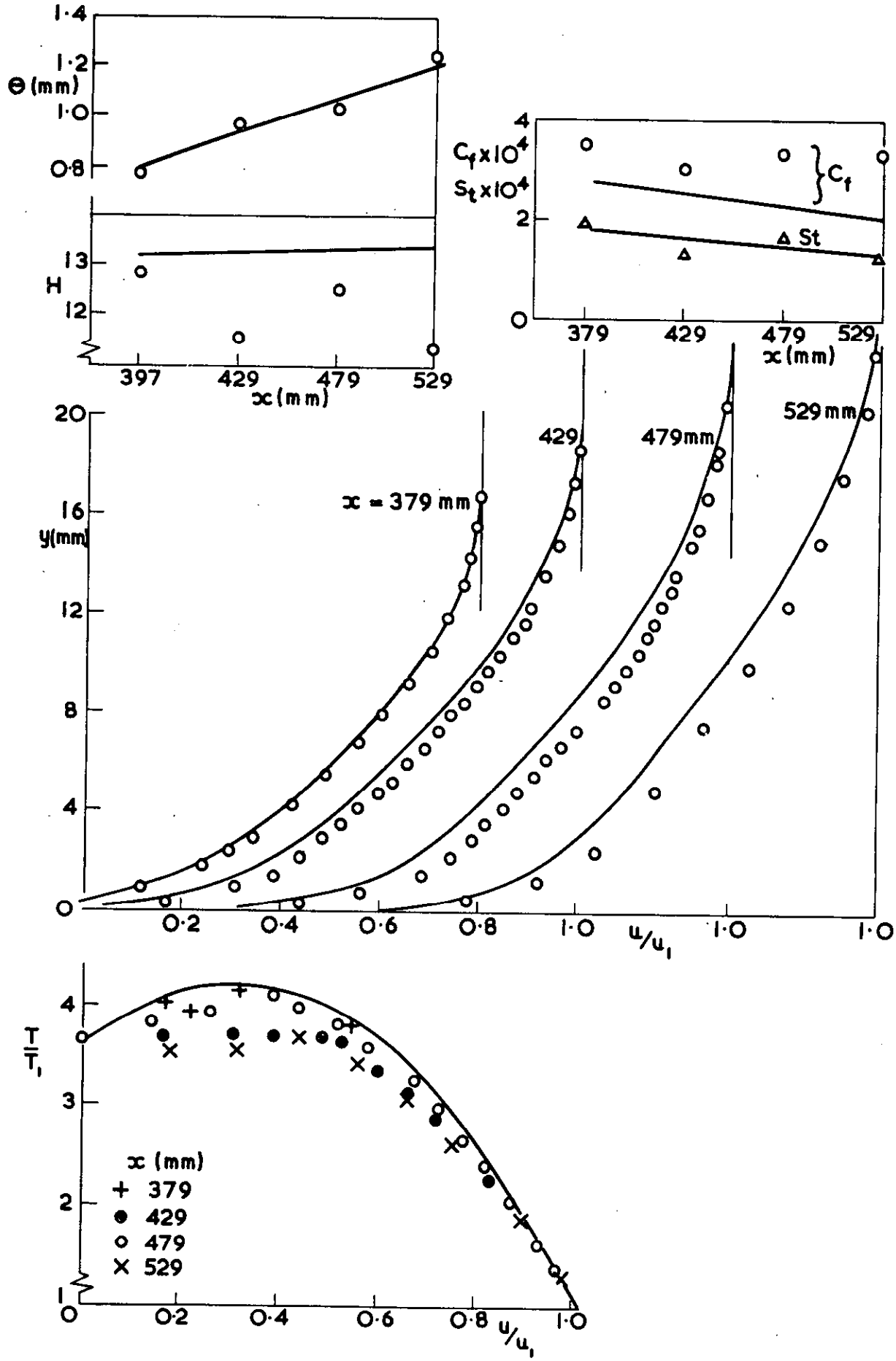

Figure 27 Results for M = 6.3, T_w/T_1 = 4, F = 0.0025. Symbols for Danberg's results.

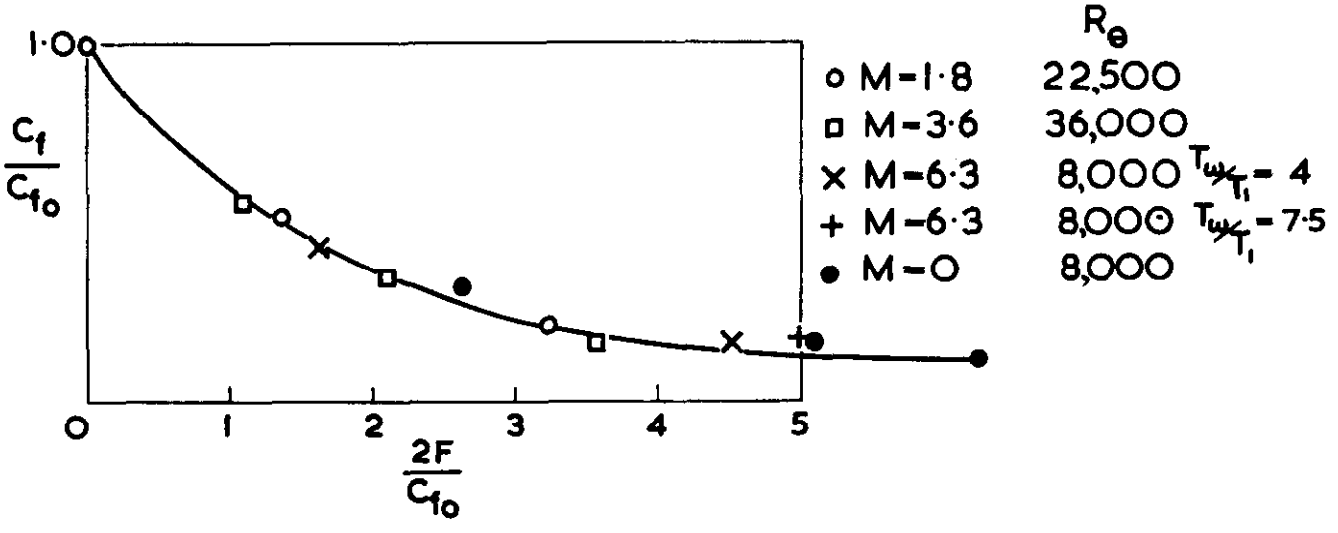

Figure 28 Calculated Variation of c_f/c_{fo} with $2F/c_{fo}$

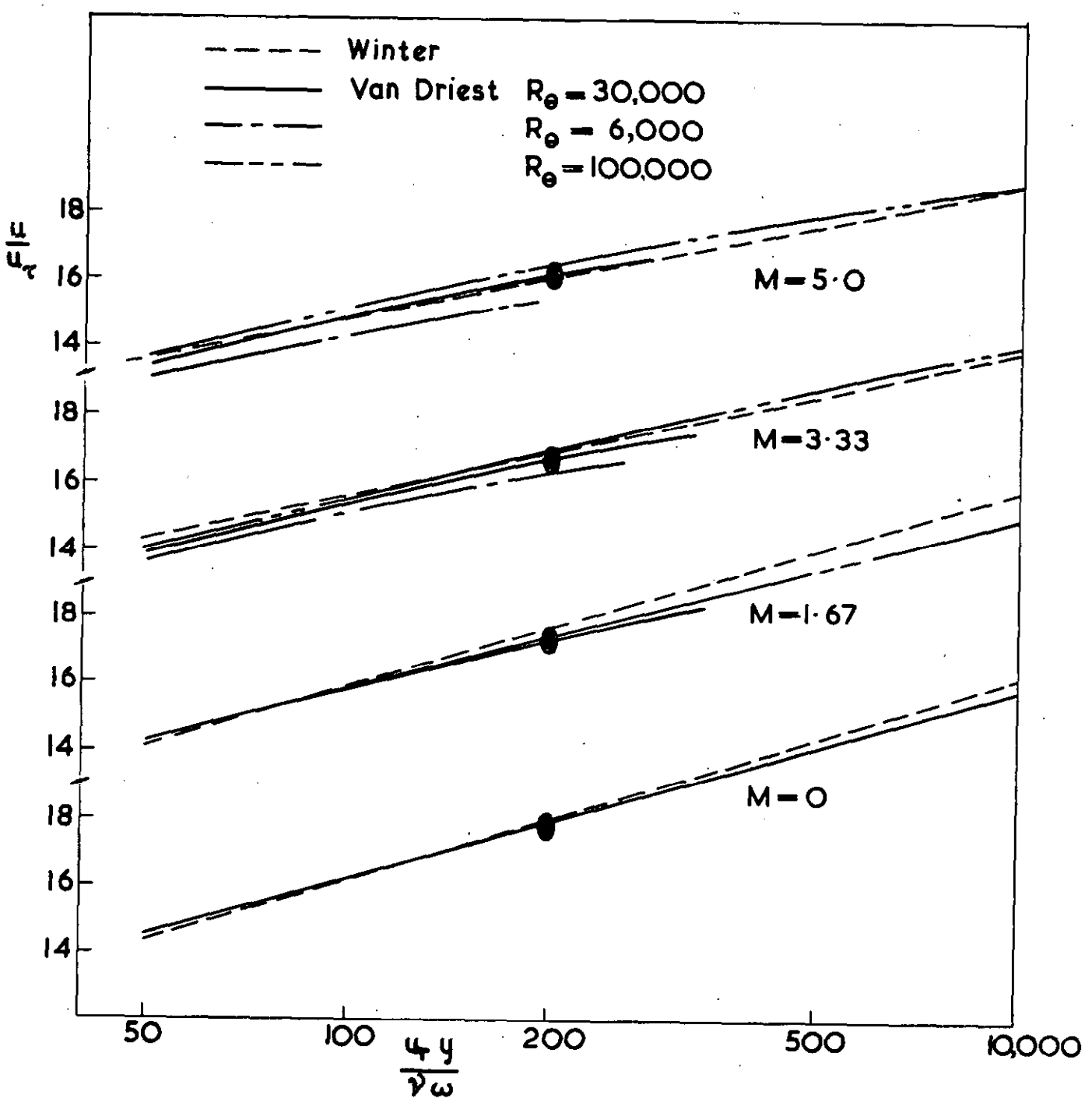

Figure 29 Law of the Wall according to Winter and Gaudet and to Van Driest

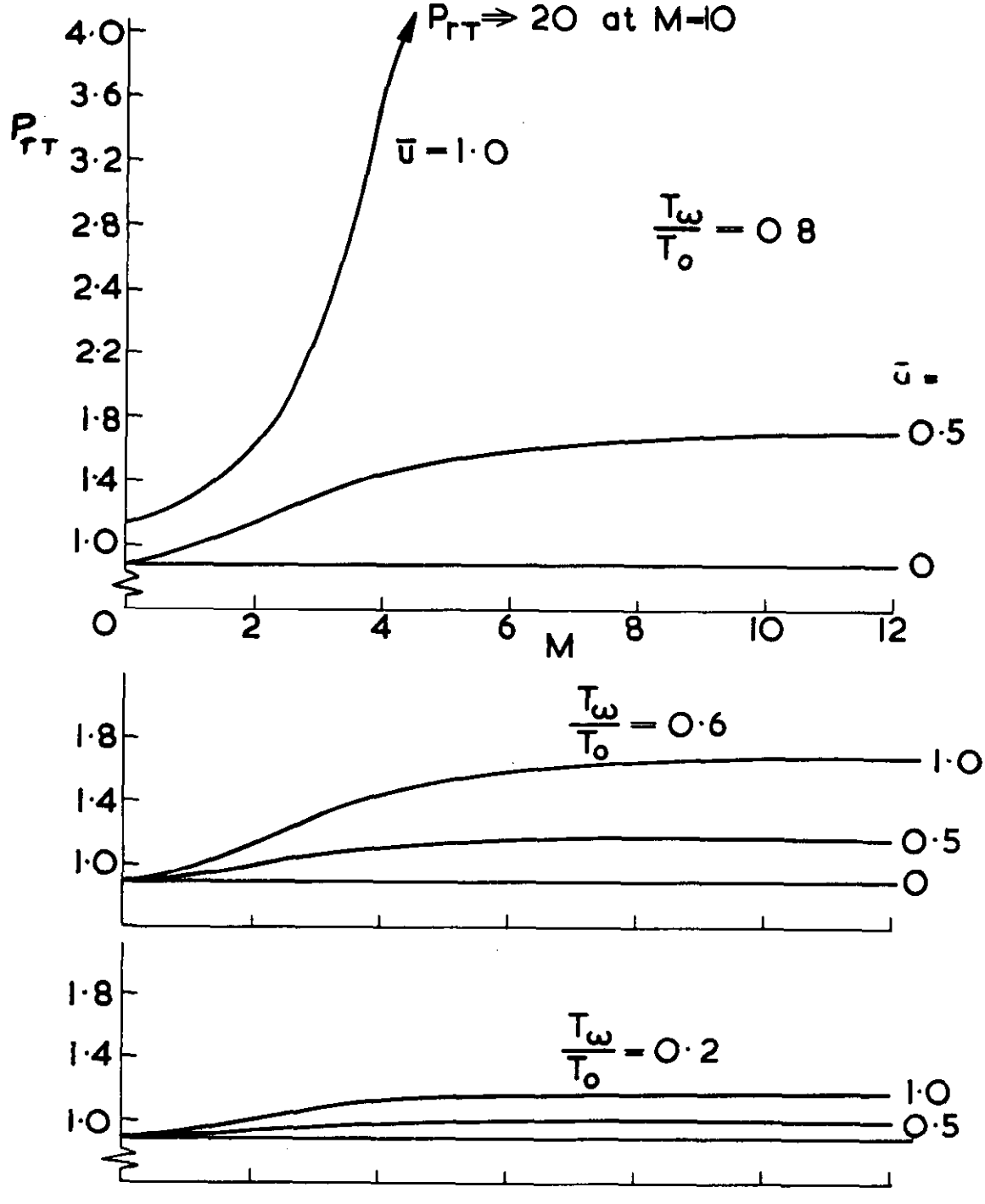

Figure 30 Variation of P_{rT} with Mach Number, P_{rt} = 0.9

DETACHABLE ABSTRACT CARDS

In comparing the calculated and experimental results emphasis has been placed on well established correlations, such as the law of the wall, the law of the wake and the Reynolds analogy factor. In spite of the scatter in the experimental data, particularly in the case of injection, it has been found that the eddy viscosity model suggested by Cebeci gives the best overall agreement with experiment at all Mach numbers.

The authors believe that, although efforts should be made to improve the calculation methods, the main requirement at the moment is for better experimental data.

In comparing the calculated and experimental results emphasis has been placed on well established correlations, such as the law of the wall, the law of the wake and the Reynolds analogy factor. In spite of the scatter in the experimental data, particularly in the case of injection, it has been found that the eddy viscosity model suggested by Cebeci gives the best overall agreement with experiment at all Mach numbers.

The authors believe that, although efforts should be made to improve the calculation methods, the main requirement at the moment is for better experimental data.

In comparing the calculated and experimental results emphasis has been placed on well established correlations, such as the law of the wall, the law of the wake and the Reynolds analogy factor. In spite of the scatter in the experimental data, particularly in the case of injection, it has been found that the eddy viscosity model suggested by Cebeci gives the best overall agreement with experiment at all Mach numbers.

The authors believe that, although efforts should be made to improve the calculation methods, the main requirement at the moment is for better experimental data.

In comparing the calculated and experimental results emphasis has been placed on well established correlations, such as the law of the wall, the law of the wake and the Reynolds analogy factor. In spite of the scatter in the experimental data, particularly in the case of injection, it has been found that the eddy viscosity model suggested by Cebeci gives the best overall agreement with experiment at all Mach numbers.

The authors believe that, although efforts should be made to improve the calculation methods, the main requirement at the moment is for better experimental data.

HER MAJESTY'S STATIONERY OFFICE

Government Bookshops

49 High Holborn, London WC1V 6HB
13a Castle Street, Edinburgh EH2 3AR
41 The Hayes, Cardiff CF1 1JW
Brazennose Street, Manchester M60 8AS
Southey House, Wine Street, Bristol BS1 2BQ
258 Broad Street, Birmingham B1 2HE
80 Chichester Street, Belfast BT1 4JY

Government publications are also available through booksellers

C.P. No. 1265

ISBN O 11 470849 5